SEMMELWEIS EGYETEM

DOKTORI ISKOLA

Ph.D. értekezések

2981.

FARKAS KLÁRA ZSUZSANNA

Bőrgyógyászat és venerológia

című program

Programvezető: Dr. Sárdy Miklós, egyetemi tanár

Témavezetők: Dr. Medvecz Márta, egyetemi docens Dr. Kiss Norbert, egyetemi tanársegéd

INNOVATIVE MULTIMODAL IMAGING APPROACHES FOR THE ASSESSMENT OF THE SKIN LESIONS IN PSEUDOXANTHOMA ELASTICUM

PhD thesis

Klára Farkas, MD

Semmelweis University Doctoral School

Rácz Károly Conservative Medicine Division

Supervisors: Márta Medvecz, MD, Ph.D.

Norbert Kiss, MD, Ph.D.

Official reviewers: Eszter Szlávicz, MD, Ph.D.

Balázs Varsányi, MD, Ph.D.

Head of the Complex Examination Committee:

Anikó Somogyi MD, Ph.D., DSc.

Members of the Complex Examination Committee:

Zsuzsanna Lengyel, MD, Ph.D.

Barbara Molnár-Érsek, Ph.D.

Budapest

2024

Table of Contents

List of Abbreviations

ABC	ATP-binding cassette
ABCC6	ATP-binding cassette protein, family C, number 6
ABI	Ankle-brachial index
AI	Artificial intelligence
AF	Autofluorescence/autofluorescent
AS	Angioid streaks
A.U.	Arbitrary units
BM	Bruch's membrane
BMP2	Bone morphogenetic protein 2
C	Cardiac
CA	Calcification area
CD	Calcification density
CARS	Coherent anti-Stokes Raman scattering
CNN	Convolutional neural network
CNV	Choroidal neovascularization
CS	Total calcification score
DR	Diffuse reflectance
DS	Dermoscopy
E	Eye
ECG	Electrocardiography
ENPP1	Ectonucleotide pyrophosphatase/phosphodiesterase 1
FOV	Field of view
G	Green wavelength band
GGCX	Gamma-glutamyl carboxylase
GI	Gastrointestinal
HFUS	High-frequency ultrasound
ICAH	Internal carotid artery hypoplasia

IFN-γ   Interferon γ

IMT   Intima-media thickness

IR   Infrared wavelength band

LED   Light emitting diode

MRP6   Multidrug resistance associated protein-6

MSI   Multispectral imaging

MPM   Multiphoton microscopy

NIR   Near-infrared

NLM   Nonlinear microscopy

NMSC   Non-melanoma skin cancer

OCT   Optical coherence tomography

PAD   Peripheral artery disease

PDE   Papillary dermal elastolysis

PET-CT   Positron emission tomography-computed tomography

PTC   Premature termination codon

PXE   Pseudoxanthoma elasticum

R   Red wavelength band

RCM   Reflectance confocal microscopy

ROI   Regions of interests

RPE   Retinal pigment epithelium

S   Skin

SHG   Second-harmonic generation

SLEB   Subepidermal low echogenic band

SRS   Stimulated Raman scattering

TGF-β   Transforming growth factor β

THG   Third-harmonic generation

TIA   Transient ischemic attack

TNAP   Tissue nonspecific alkaline phosphatase

TNF-α   Tumor necrosis factor α

TPEF   Two-photon excitation fluorescence

UE	Ultrasound elastography
V	Vascular
18F-NaF	18F-Sodium Fluoride

1. Introduction

1.1 Imaging techniques in dermatology

The utilization of imaging modalities in dermatology has emerged as an essential part of clinical care in the diagnosis and management of various skin disorders [1,2]. Imaging modalities facilitate the visualization of cutaneous and subcutaneous structures, thus leading to more accurate diagnoses, superior treatment planning, and improved monitoring of disease progression. Considering the clinical application of imaging methods, crucial features encompass portability, bedside feasibility, user-friendliness, time efficiency, noninvasive, high-resolution imaging, real-time output, and cost-effectiveness. With the use of novel imaging devices, skin biopsy would be required less frequently and - in addition to dermoscopic images - additional information could be obtained [3,4].

1.1.1 Dermoscopy

Dermoscopy (DS) is a widely used handheld device in the field of dermatology. DS is an epiluminescence microscope with 10x magnification, that can be used to visualize characteristic features of the epidermis and superficial papillary dermis.

DS can be used with non-polarized mode which allows better visualization of certain superficial structures, such as milia-like cysts in seborrhoeic keratosis, or with polarized mode which allows visualization of deeper vascular structures.

In addition to its use in the diagnostics of melanocytic lesions, DS has been used to examine a wide range of skin diseases of various etiologies, including genodermatoses [5].

Videodermoscopy can capture images in high resolution and store images of skin lesions for detailed analysis and comparison over time. The high magnification capabilities provide advantages beyond improved visualization, as it is a valuable tool for educational purposes [6].

1.1.2 High-frequency ultrasound (HFUS)

In dermatological practice, multi-frequency ultrasound scanning methods (ranging from 15-22 MHz) with linear or hockey stick transducers are frequently utilized. These techniques, such as real-time ultrasound, fine flow, color Doppler, and shear wave tissue elastography can provide highly precise descriptions of skin morphology [3].

Application of these techniques is clinically useful in both malignant and benign skin lesions. In case of malignant melanoma, the Breslow tumor thickness can be predicted by HFUS, thus the pre-operative US scanning can determine the surgical margins [7]. Previous studies have shown that in many cases, skin tumor thickness can be assessed using ultrasound with a resolution of 10-20 Mhz, which is widely available [8]. In the case of basal cell carcinoma, HFUS allows the differentiation of several subtypes [9]. In cutaneous lymphoma, ultrasound technique has an important role in diagnosis and follow-up. In many connective tissue diseases, such as scleroderma or systemic lupus erythematosus, the fibrotic tissue can be analyzed by ultrasound elastography (UE) [10]. Inflammatory skin diseases (e.g., atopic dermatisis, psoriasis) show characteristic HFUS morphology: hypoechogenic band is seen in the subepidermal area (SLEB =subepidermal low echogenic band), and colour Doppler shows increased blood flow. Skin HFUS examination is recommended in hidradenitis suppurativa to confirm the diagnosis, determine the clinical stage and monitor the efficacy of therapy [11].

1.1.3 Optical coherence tomography (OCT)

The first study about optical coherence tomography used in skin diseases was reported in the late 1990s [12].

OCT uses infrared (IR) or near-infrared (NIR) radiation, which allows higher resolution (3 µm), but the captured area and depth are less than in ultrasound images. In addition to cross-sectional images, novel OCT equipment can acquire horizontal and 3D images as well. It provides 2 mm penetration; thus, epidermis and dermis can be examined. OCT can be used for the diagnosis of melanoma and non-melanoma skin cancer (NMSC) and can assist in preoperative planning of surgical margins [13,14]. OCT has also been successfully used to investigate nail diseases (nail psoriasis and onychomycosis), inflammatory skin diseases (contact dermatitis and seborrhoeic dermatitis), autoimmune blistering skin diseases, vascular lesions (nevus flammeus

and hemangioma), acne and rosacea, and skin lesions associated with fibrosis (systemic sclerosis and scars) [15,16].

1.1.4 Confocal microscopy

The *in vivo* confocal microscope which is utilized in dermatology is the reflectance mode confocal microscopy (RCM) device, using a NIR laser light of 830 nm wavelength and a power of less than 15 mW. The obtained images display in grey-scale, horizontal dimension of epidermis and papillary dermis. The images can be acquired in small fields of view, usually 0.5 x 0.5 mm^2, and then merged into mosaic images to provide a view of up to 8 x 8 mm^2. RCM provides cellular resolution (0.5-1.0 µm) and is therefore suitable for visualizing the histological structures of skin lesions [17,18].

The main indications for the use of RCM is the *in vivo* diagnosis of various skin cancers and inflammatory skin diseases (e.g., psoriasis, lupus erythematosus and contact dermatitis). In case of uncertain clinical and dermoscopic diagnoses, RCM is recommended to improve diagnostic accuracy. It can play an important role in the presurgical estimation of skin tumors margins, can be used to detect recurrent cancers and to monitor efficacy of topical therapies.

However, RCM technique is limited by the fact that it does not allow imaging deeper than 200 µm, the cost of the microscope is very high compared to dermoscopy and it is time consuming. The penetration depth is limited by significant hyperkeratosis, erosion or ulceration and in many cases vascular structures cannot be visualized as they are located too deep. The localization (e.g., palm, sole, not accessible area), and shape (nodular) of the lesions cause difficulties during the examination. [18]. Compared to RCM, OCT equipment can display a larger field of view, provide deeper tissue penetration and have a 3D mode [19].

1.1.5 Multiphoton microscopy (MPM)

In MPM, also known as nonlinear microscopy (NLM), two or more photons excite the molecules. Fluorophores are excited by two or more photons of low energy in the near-infrared spectrum. Ultrashort pulsed laser sources are required to generate NLM signal. Laser intensities are concentrated in time and space: with the use of femtosecond lasers, the laser beams are

focused into a volume of approximately 1 μm^3 in size. As a result, molecules outside this volume are not excited [20].

NLM techniques can be grouped according to the number of laser beams used. One laser beam is needed for two-photon excitation fluorescence (TPEF), second-harmonic generation (SHG) and third-harmonic generation (THG) excitation. Two laser beams are required for the modalities of coherent anti-Stokes Raman scattering (CARS) and stimulated Raman scattering (SRS) [21,22].

While conventional microscopy achieves a penetration depth of about 100 μm due to high scattering, NLM techniques may provide a maximum depth of 400-500 μm [23].

One of its main advantages is the ability to scan the skin without staining, providing noninvasive visualization and high-resolution images of the skin [24,25].

The skin is an excellent target for NLM techniques, providing detailed morphological information about its main components, such as endogenous fluorophores/protein structures such as NAD(P)H, flavins, keratin, collagen, elastin, porphyrins, and melanin, which give high signal when using NLM [21,26].

NLM has been previously utilized *ex vivo* and *in vivo* in mice to investigate the effects of obesity on dermal tissues, various types of diet-induced obesity and connective tissue changes after physical exercise [27-29].

In human, it has been previously utilized *ex vivo* for the imaging of malignant skin tumors [30,31], and rare inherited skin disorders (e.g., Fabry disease [32], keratinopathic ichthyosis [33], Ehlers -Danlos syndrome [34] and PXE [35]).

1.2 Pseudoxanthoma elasticum (PXE)

Pseudoxanthoma elasticum (PXE, OMIM#264800, ORPHA:758) is a rare, multisystemic disorder which belongs to the inherited connective tissue diseases, notably to the elastinopathies. Characteristics skin symptoms were observed in 1881 by *D. Rigal*, and 15 years later *F-J* [36,37]. *Darier* coined the term pseudoxanthoma elasticum. In 1992, *E. E. Grönblad* ophtalmologist and *J. V. Strandberg* dermatologist revealed the association between the skin and ocular manifestations, therefore PXE is also known as Grönblad-Strandberg syndrome [38,39].

1.2.1 Epidemiology

The estimated prevalence of PXE is between 1:25.000 and 1:50.000, with a predominance of female patients (female to male ratio of 2:1) [40]. Regarding the worldwide epidemiological data, there are ~200-400 PXE patients in Hungary [41]. It was observed that the cutaneous involvement was more severe among female patients, while the cardiovascular complications are more common among the male patients [42].

1.2.2 Etiology and pathophysiology

PXE is an autosomal recessive inherited connective tissue disorder. In 2000, it was proven that PXE is caused by mutations in the *ABCC6* (ATP-binding cassette protein, family C, number 6) gene, which encodes the C6 subunit of the human ABC (ATP-binding cassette) transporter, also known as the MRP6 (Multidrug resistance associated protein-6) [43]. The *ABCC6* gene is located on chromosome 16p13.11, which consists of 31 exons. It is mainly encountered in the liver on the basolateral surface of hepatocytes and in the kidney, but it also occurs in small amounts in the connective tissue of the skin, retina and blood vessels. To date, more than 350 pathogenic variants have been identified in the *ABCC6* gene that leads to PXE [44]. Nonsense, missense mutations, deletions, insertions and splice-site mutations were also detected. The two most common mutations are the p.R1141X nonsense mutation, which occurs in ~30% of PXE patients and the mutation in exons 23-29 deletion (EX23_29del), which was detected in 20% of the American population and 12% in Europe. In Hungary, the p.R1141X mutation has a 30% prevalence in PXE patients [35], which, based on literature data, is considered an increased risk

factor for cardiovascular manifestations and increases the risk of developing early coronary disease [45,46]. The severity of ocular and vascular manifestations increases with the degree of loss of *ABCC6* gene function. In cases with complete loss of function, the risk of retinal bleeding is high, and severe claudication requiring vascular surgery may also develop [42].

The role of the ABCC6 transporter has not been completely described. Since, its expression is very low in tissues affected by PXE, it was assumed that ABCC6 expressed in the liver being responsible for the peripheral tissue involvement, as hepatocytes produce 60% of inorganic pyrophosphate (PPi), which is an important antimineralization factor. Mutations in the *ABCC6* gene lead to decreased ATP release in the hepatocytes, hence the serum level of PPi will be lower. Therefore, deposits of calcium salts (calcium hydroxyapatite, calcium hydrogen phosphate) develop in the skin, in the eyes and in the cardiovascular system [47,48].

The reduced PPi level is not the only factor responsible for the connective tissue alterations characteristic of the disease. The altered expression of TGF-β and BMP2 (bone morphogenetic protein 2) and its effect on signaling pathways, the fact that TNF-α and IFN-γ reduce *ABCC6* promoter activity, and the role of proinflammatory cytokines as mediators of vascular calcification are also being investigated [49,50].

In addition to the *ABCC6* gene, ENPP1 (Ectonucleotide Pyrophosphatase/Phosphodiesterase 1) and GGCX (gamma-glutamyl carboxylase) mutations can also cause similar phenotypes to PXE. Because of the remarkable resemblance to PXE, it is called PXE-like disease (OMIM 610842).

Furthermore, modifier genes can affect the metabolism of plasma PPi and play a role in ectopic mineralization [51]. Expanding the knowledge of the genetic and molecular complexity can lead us one step closer to understanding the phenotypic variability of PXE. By identifying the modifier genes, we may be able to more accurately estimate the progression of the disease.

1.2.3 Clinical findings

PXE shows clinically heterogenous symptoms. The severity of the diseases, the involvement of the organs, the extension and progression of the symptoms, and the age of onset display individual variability. Pathological changes primarily affect the skin, eyes and cardiovascular system. In rare cases, gastrointestinal bleeding and kidney involvement may also develop.

1.2.4   Cutaneous manifestations

The first lesions appear on the skin as small, 1–5 mm yellow papules and plaques (which may mimic xanthomas) on the predilection area, most frequently on the neck or on the flexural areas such as on the axillar region, on the wrist, on the inguinal area or on the popliteal regions, but it can affect the periumbilical region as well (Figure 1). In rare cases, these symptoms can also occur on the mucous membrane of the mouth, vagina and rectum. Later, the papules coalesce into plaques and the lesions affect an increasingly larger skin area and continue to develop on several skin sites. As a consequence of the fragmented elastic fibers, the skin loses its elasticity and becomes lax and redundant.
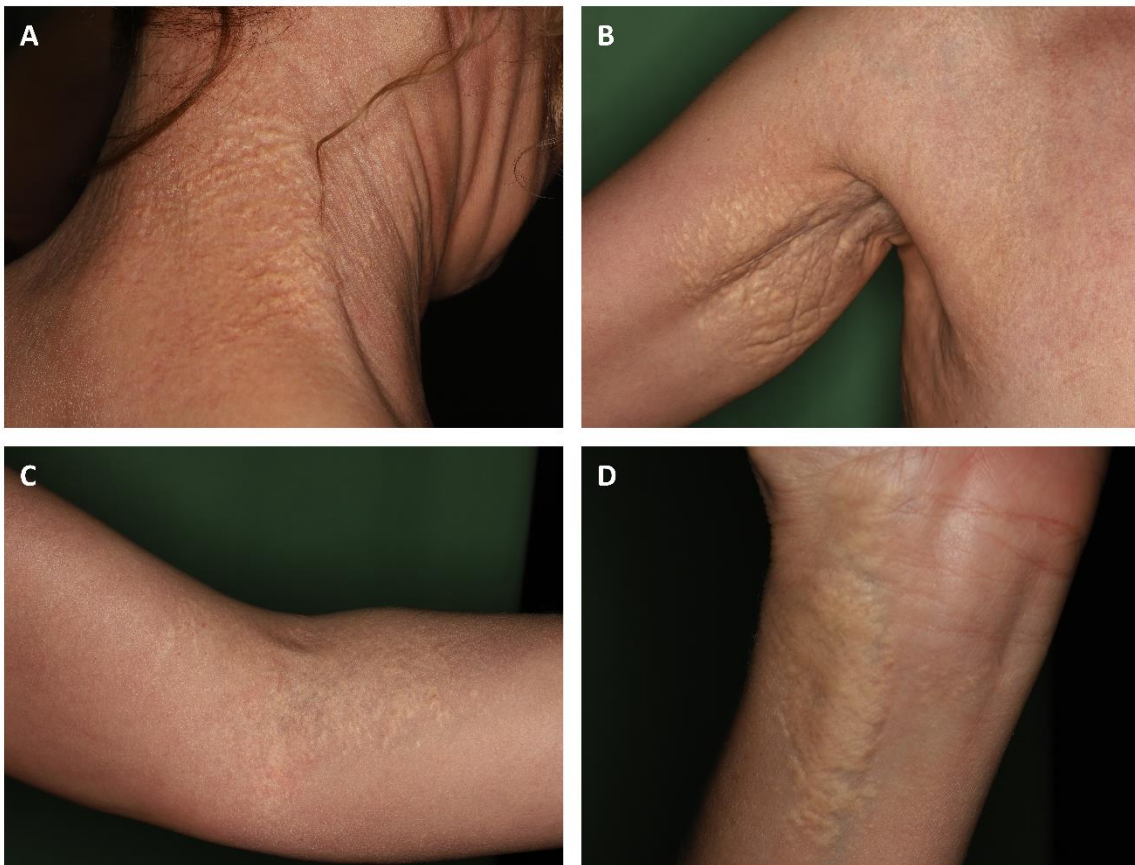

Figure 1. Typical cutaneous lesions in pseudoxanthoma elasticum A) 3-5 mm yellow papules and plaques on the posterolateral side of the neck B) white plaques and loose, redundant skin on the axilla C) 2-3 mm yellowish-white papules and plaques on the antecubital fossa D) 3-4 cm yellowish-white coalesced plaques on the wrist. (Semmelweis University, Department of Dermatology, Venereology and Dermatooncology)

1.2.5   Ocular manifestations

The quality of life in PXE patients is affected especially by vision impairment. Because of that fact, the patients most commonly seek medical consultation upon experiencing ocular symptoms, accordingly, ophthalmologists play a decisive role in the diagnosis of PXE [52].

Peau d'orange is most often the first ocular alteration, which appear as a diffuse mottling of the retinal pigment epithelium (RPE). It has been hypothesized that peau d'orange is a sign of microcalcification of Bruch's membrane (BM) and it causes no visual impairment (Figure 2/A) [52].

The fragmentation and calcification of the elastic fibers lead to ruptures in Bruch's membrane and irregular lines of varying thickness, referred to as angioid streaks (AS) appear concentrically around the optic nerve (Figure 2/A). Depending on the degree of RPE atrophy, AS displays red, light or dark brown lines. The main complication of AS is the subretinal choroidal neovascularization (CNV), which develops in 72–86% of cases and it is bilateral in more than 70% of cases [53]. However, AS itself does not cause visual acuity loss, even if the fovea is affected, but the resulting developed CNV, oedema, subsequent fibrosis and scarring lead to significant loss of vision (Figure 2/B) [52].

Bright spot-like structures ("comet") and comets with a tail pointing toward the optic nerve head ("comet tails") may appear on the periphery of the retina. Comets and comet tails are unique pathognomonic features of PXE. Abnormal mineralization of the lamina cribrosa leads to development of drusen (hyaline nodules) in the area of the optic nerve [52].
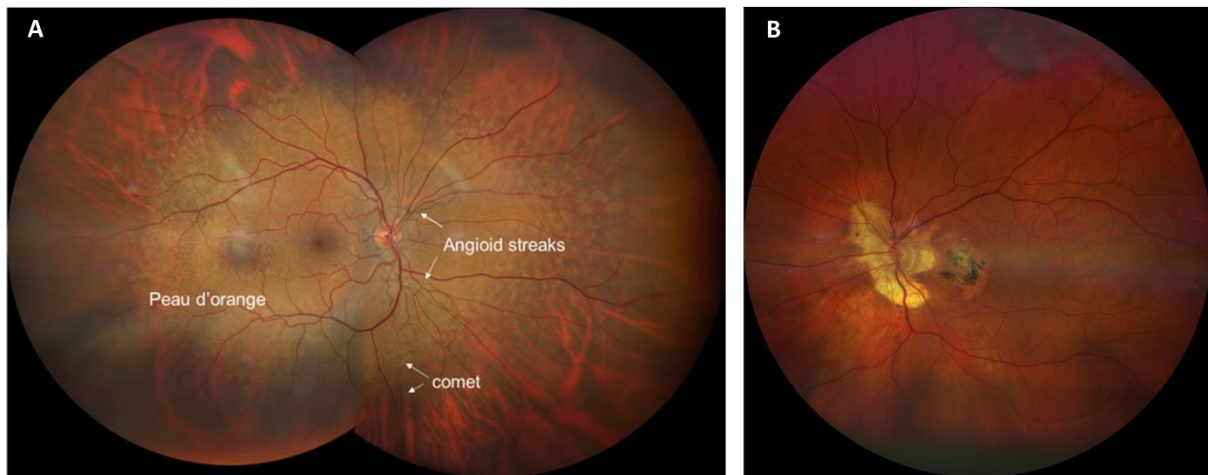
Figure 2. Fundus abnormalities in pseudoxanthoma elasticum (PXE) A) Collage photograph of the fundus of a young, 33-year-old male patient with PXE, B) Fundus photograph of a 51-year-old female patient with PXE, showing pigmented scar tissue in the macula, brownish angioid streaks (AS) and atrophy around the papilla, hyperreflective comet and comet tails lesions in the peripheral area of the retina. (Semmelweis University, Department of Ophthalmology)

1.2.6 Cardiovascular manifestations

Patients with PXE have an increased risk of cardiovascular disease because of the vascular morphological changes. The mineralization and fragmentation affect the elastic fibers of the internal elastic lamina and adventitia in the aorta and medium-sized arteries, the intramyocardial arterioles and epicardial coronary arteries. Similar changes have been described in the endocardium and epicardium [54,55]. Accumulations of proteoglycans in tunica media of the arterial wall - which attract calcium - lead to thickening of the artery wall [55] (Figure 3). Early atherosclerosis can develop often in the internal carotid artery but in a previous study, it was found, that atherosclerosis occurs frequently in the lower extremities [56]. Cardiovascular manifestations occur as hypertension, claudication intermittent, ischemic stroke and gastrointestinal bleeding caused by peripheral vascular disease. In PXE patients, the most common coronary artery diseases are the angina pectoris and myocardial infarction [45,56-58]. In addition, the early onset of left ventricular diastolic dysfunction has also been described [59]. Renal artery narrowing can lead to secondary hypertension [60]. Although PXE patients typically have a normal life span, case series have been reported on myocardial infarctions and sudden cardiac death in the teens or twenties [54]. It is unlikely that cardiological manifestations are the first clinical signs of PXE, but in a young patient suffering from cardiovascular diseases
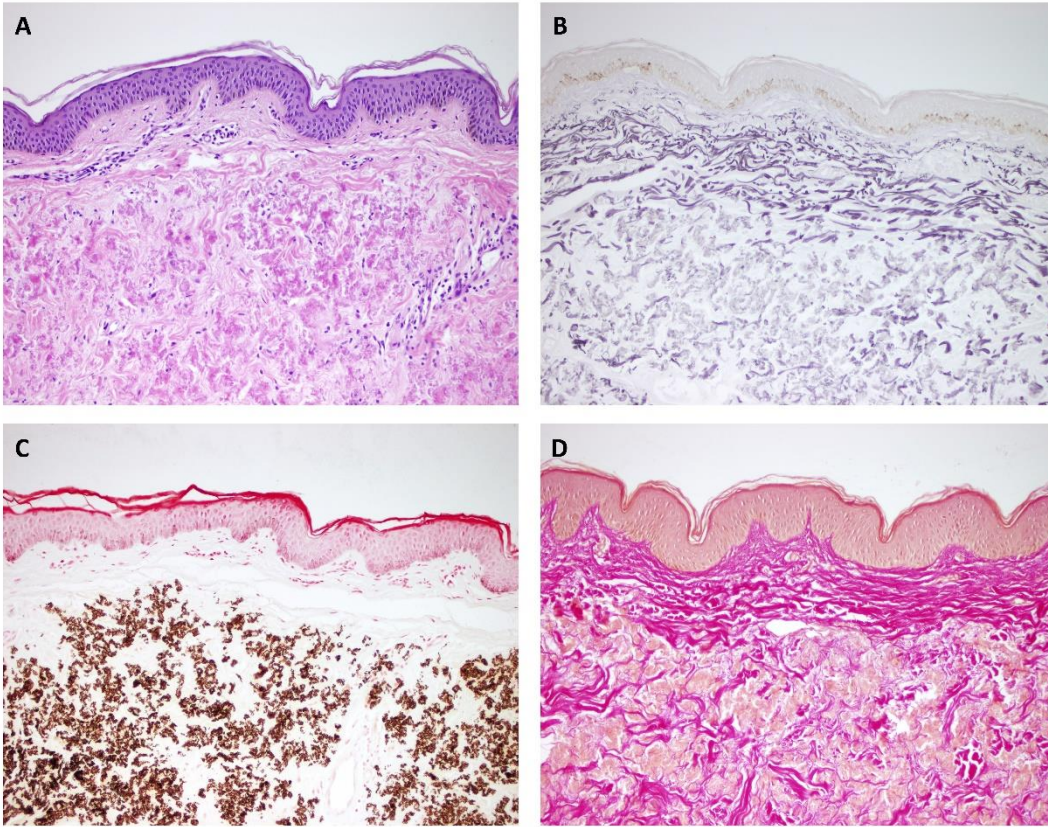
without any risk factors, PXE should also be considered [61]. It has also been reported that not only PXE patients have an increased risk of cardiovascular complications, but also the heterozygous carriers of *ABCC6* mutations [45,56].

Figure 3. Cardiovascular manifestations in patients with pseudoxanthoma elasticum A) and C) Specific small calcification in the subintimal region (blue arrow) B) Increased intima-media thickness (IMT), 1.01mm D) Decreased mitral annular tissue Doppler velocities in an otherwise healthy 51-year-old patient with PXE. (Semmelweis University, Heart and Vascular Centre)

1.2.7   Diagnosis

Although the skin lesions are characteristic in their appearance and location, the diagnosis can be confirmed through a skin biopsy.

The typical histological features of PXE can be observed with the use of specific stains by light microscopy. Fragmented elastic fibers are shown by hematoxylin-eosin staining or by Weigert's elastic staining which is specific for elastic fibers. Von Kossa staining reveals mid-dermal salt deposits and van Gieson stains the abnormal collagen fibers [62] (Figure 4).

Figure 4. Histopathological characteristics of pseudoxanthoma elasticum A) with hematoxylin and eosin, B) Weigert's elastic staining for elastin, C) von Kossa staining for calcium deposits, and D) van Gieson staining for collagen. 100x magnification. (Semmelweis University, Department of Dermatology, Venereology and Dermatooncology)

The current guidelines for diagnostic criteria of PXE were developed by *Plomp et al.* in 2010. The criteria system is established based on dermatological, ophthalmological and genetic examination, according to major and minor criteria (Table 1) [63].

Table 1. Diagnostic criteria for pseudoxanthoma elasticum (PXE) created by *Plompt et al.* [63].
Definitive diagnosis: The presence of two (or more) major criteria not belonging to the same (skin, eye, genetic) category.
Probable diagnosis: The presence of two major eye or two major skin criteria or the presence of one major criterion and one or more minor criteria not belonging to the same category as the major criterion.
Possible diagnosis: The presence of a single major criterion or the presence of one or more minor criteria.

Major diagnostic criteria	Minor diagnostic criteria
1. Skin a. Yellowish papules and/or plaques on the lateral side of the neck and/or flexural areas of the body; or b. Skin biopsy: fragmented, clumped and calcified elastic fibers.	*1. Eye* a. One AS shorter than one disk diameter; or b. One or more 'comets' in the retina; or c. One or more 'wing signs' in the retina
2. Eye a. Peau d'orange; or b. Angioid streaks (at least as long as one disk diameter)	*2. Genetics* a. A pathogenic mutation of one allele of the *ABCC6* gene
3. Genetics a. Pathogenic mutation of both alleles of *ABCC6* gene b. A firs-degree relatives with definitive PXE diagnoses	

The Phenodex score assesses the severity of the organ affection and based on the severity of symptoms affecting the skin (S), eye (E), gastrointestinal (GI), vascular (V) and cardiac (C) patients can be assigned a severity number. It can be used to monitor the clinical phenotype of PXE patients. This system was expanded with other cardiac and vascular symptoms, neurological information and nephrological manifestations by *Legrand et al* (Phenodex+ score) (Table 2) [42].

Table 2. Phenodex+ score for phenotype classification of patients with pseudoxanthoma elasticum (PXE).

EKG: electrocardiogram; TIA: transient ischemic attack

Skin

S0	No symptoms
S1	Papules
S2	Plaques
S3	Lax, redundant skin

Eye

E0	no symptoms
E1	Peau d' orange
E2	Angioid streasks
E3	Belleding and/or scars

Gastrointestinal

GI0	no symptoms
GI1	Gastrointestinal bleeding as related to PXE

Vascular

V0	no symptoms
V1	Weak or absent pulse or peripheral artery disease revealed by vascular imaging
V2	Intermittent claudication
V3	Vascular surgery or Stroke/TIA

Cardiac

C0	No symptoms
C1	Chest pain/angina/abnormal EKG or abnormal stress test with no symptom, or mitral insufficiency
C2	Heart attack

Renal

R0	No symptoms
R1	Nephrolithiasis

1.2.8   Imaging methods in PXE

During the dermatological examination, in addition to the characteristic clinical presentation, DS as a non-invasive examination method can also help establish the diagnosis of PXE. However, only a few studies have been published on the dermoscopic features of PXE. The characteristic multiple irregular yellowish areas and superficial linear vessels were described first in 2017 by *Lacarrubba et al*. [64]. The variant arrangements of the yellowish clods were reported in detail by *Berthin et al*. The pattern of the yellowish globules present themselves as dots, parallel lines, plaques, irregular broad or narrow mesh network [65] (Figure 5). The vessels can be linear or reticulated or can be absent. *Kawashima et al*. suggested that the color of the background is caused by the mid-dermal vasodilation. It can appear as purple, red, pink or brownish color. It was noted, that the dermoscopy can help with differential diagnoses between PXE and PXE-like papillary dermal elastolysis (PDE), because the background and the clods are displayed in a lighter color in PXE-like PDE [66].

| Dots and reticular vessels | Dots/ Linear pattern | Parallel lines |
| Plaque of coalesced papules | Broad mesh network | Narrow mesk network |
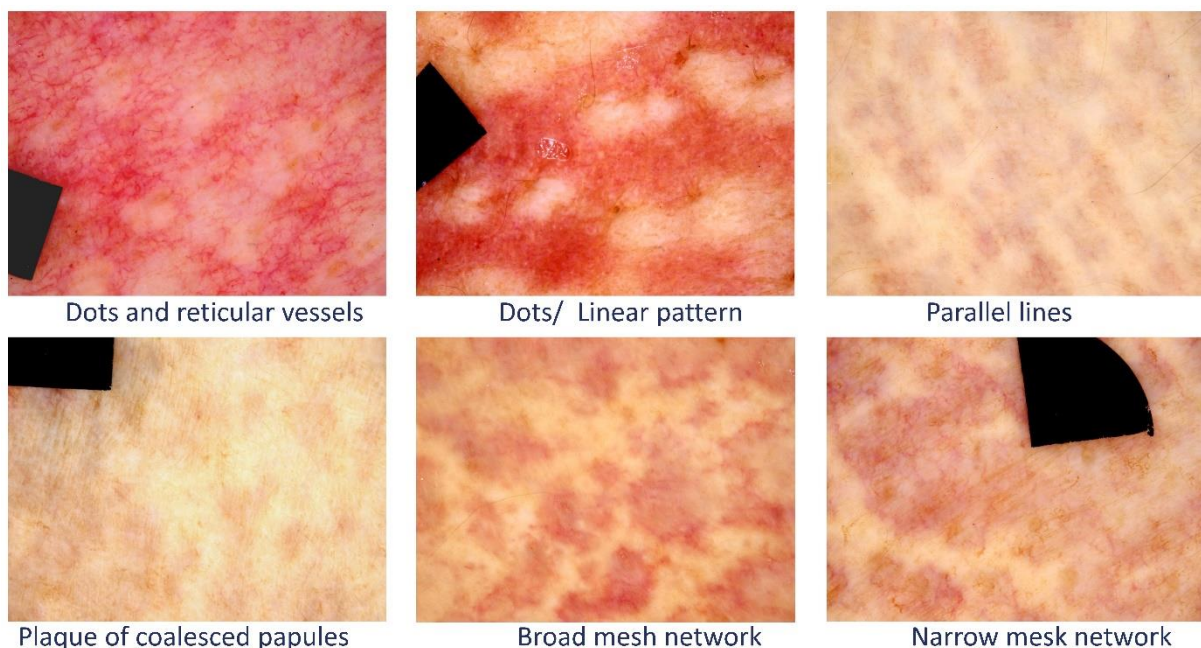
Figure 5. Our dermoscopic images of cutaneous manifestations in pseudoxanthoma elasticum (PXE). The arrangement of yellow globules grouped according to the nomenclature of Berthin C. at. al. [65]. Black markers are used for image alignment. (Semmelweis University, Department of Dermatology, Venereology and Dermatooncology)

There are various other non-invasive techniques to detect certain characteristic skin changes in PXE patients. These include HFUS, RCM and OCT [67-69]. Furthermore, it was reported that

positron emission tomography-computed tomography (PET-CT) is able to detect inflammation and calcification in PXE-affected skin sites.

Ex vivo NLM technique provides high-resolution imaging of the specific histopathological features of PXE-affected skin. We can visualize elastin and calcium deposits by using TPEF and the collagen fibers by using SHG techniques [35].

1.2.9 Differential Diagnosis

Generalized arterial calcification of infancy (GACI) shows serious, systemic clinical symptoms and skin hyperlaxity. These skin manifestations are similar to those observed in PXE. Skin symptoms resembling PXE can appear in many other hereditary and acquired dermatological disorders: cutis laxa, Ehlers-Danlos syndrome, solaris elastosis, fibroelastolytic papulosis and dermal elastolysis [70].

Angioid streaks can develop not only in PXE. Apart from PXE, retinal angioid streaks can also occur in Marfan syndrome, Ehlers-Danlos syndrome, Paget's disease, acromegaly, hematological diseases (sickle cell anemia, thalassemia, spherocytosis) and other pathologies [71].

1.2.10 Management

In some cases, where the skin symptoms worsen the quality of life, plastic surgery may be necessary. If the lesions are milder and localized, satisfying cosmetic results can be achieved with fractional carbon dioxide laser. In a previous Hungarian publication, the possible efficacy of the local corticosteroid and cryotherapy was mentioned [72,73].

Treatment of ophthalmological manifestations

Ocular involvement can lead to blindness if it is left untreated, but with prompt therapy, the progression of symptoms can be reduced and prevented. CNV can be effectively managed with intravitreal vascular endothelial growth factor (VEGF) inhibitor (e.g., bevacizumab, ranibizumab) treatment, however, the localization of the pathological neovascularization significantly affects the prognosis. Other therapeutic options include photodynamic therapy, laser photocoagulation, transpupillary thermotherapy, and macular translocation surgery. Patients with AS must be protected from trauma of the head and eyes in order to decrease the

risk of choroidal rupture. It is recommended to wear protective glasses while doing sports or working and contact sports should be avoided [74,75].

Management of cardiovascular manifestations

In PXE patients, it is extremely important to reduce cardiovascular risk factors by following a suitable lifestyle (avoid smoking, weight control, regular exercise, etc.). In the case of an abnormal lipid profile or hypertension, when the discrepancy cannot be resolved with lifestyle changes, pharmacological treatment is crucial [76].

Although causal therapy for PXE is currently not available, when establishing the diagnosis, both homozygous and heterozygous carriers are recommended to undergo cardiological/angiological screening (blood pressure, laboratory tests, echocardiography, ankle-brachial index (ABI), carotid and extremity duplex ultrasound), to start appropriate preventive steps. In addition, a fecal blood test is also recommended, especially in the case of abdominal complaints [56,77].

It should be emphasized that the routine use of acetylsalicylic acid for preventive purposes is not recommended in PXE patients due to the increased risk of retinal and GI bleeding [76].

In case of intermittent claudication, weight loss and a targeted physiotherapy can help by stimulating collateral circulation. Above the age of 40, the introduction of physiotherapy is also recommended for preventive purposes. Pentoxyphilline treatment may be beneficial but is not recommended in case of recent retinal or GI bleeding. In severe arterial stenosis, percutaneous angioplasty or bypass surgery can be performed, although this is rarely necessary [78].

Causal therapeutic approaches and perspectives on personalized medicine

Antimineralization therapies

In some clinical studies, the efficacy of aluminum hydroxide, sevelamer hydrochloride, disodium pyrophosphate and the beneficial effect of magnesium intake were investigated, which reduce ectopic mineralization, so that fewer hydroxyapatite crystals develop in the body. In PXE, etidronate and intravenous sodium thiosulfate can be effective for systemic arterial calcification, the latter also improves skin symptoms [79,80].

Experimental animal models

Oral tetrasodium pyrophosphate showed antimineralization properties in Abcc6 −/− mice. Cholesterol-lowering drugs such as atorvastatin can reduce the extent of ectopic mineralization. Inhibition of tissue nonspecific alkaline phosphatase (TNAP) with SBI-425 increases plasma PPi levels, thus reducing pathological tissue mineralization. With ENPP1 enzyme replacement therapy, normalization of the plasma PPi level was achieved, which prevented ectopic mineralization. Intravenous inositol hexaphosphate (INS-3001) and myo-inositol hexaphosphate (SNF472) selectively inhibit the formation of hydroxyapatite [81].

Allele-specific and gene therapy modalities

The importance of accurate genetic testing of PXE patients is emphasized by the preclinical allele-specific therapeutic studies. Regarding some missense mutations, the allele-specific chaperone therapy options ensure the correction of the intracellular trafficking of the abnormal protein. In the case of a common nonsense mutation resulting in an early stop codon, the non-aminoglycoside premature termination codon (PTC) "read-through" suppressor agent labeled PTC124 facilitates the translation [82].

Functional, additive *ABCC6 in vivo* gene therapy transferred by adenovirus vector was performed in murine animal model, however the efficacy was limited by its immunological effects. In the future, further extensive preclinical and clinical studies are needed to confirm the results [83].

2. Objectives

The present study aims to introduce novel imaging techniques for the assessment of the skin lesions of patients with PXE and to reveal the association between the extension of PXE skin lesions and systemic involvement.

I. Study

I/ 1. We aimed to evaluate the *in vivo* visualization of the characteristic skin changes in PXE.

I/ 2. We aimed to visualize the characteristic dermoscopic features with multispectral imaging (MSI) device.

I/ 3. It has been hypothesized that with the help of a MSI device using autofluorescence (AF) light we can observe and measure the calcified areas of the PXE-affected skin.

I/ 4. Quantification and comparison of the intensity of the images on the PXE-affected and on the healthy skin areas.

II. Study

II/ 1. Furthermore, we aimed to explore the association between the extension of the skin manifestations and the severity of the systemic involvement.

II/ 2. We aimed to evaluate the skin involvement objectively and quantitatively.

II/ 3. We attempted to assess skin severity by the extent of ectopic calcification in the skin using *ex vivo* NLM.

II/ 4. We aimed to create parameters which can be used to determine the amount of skin calcification.

II/ 5. We investigated the correlation between the calcified area in the skin and different systemic involvement.

3. Methods

3.1 Patient data

3.1.1 I. Study

We examined five patients (three female and two male patients) with a mean age of 55 ± 8.1 years using AF and diffuse reflectance (DR) imaging with narrow-band light emitting diode (LED) excitation. All these patients were diagnosed and managed with PXE at Semmelweis University, Budapest, Hungary. The diagnosis was based on the revised diagnostic criteria of PXE [63]. The diagnosis of PXE was verified by molecular genetic analysis of the *ABCC6* gene in all patients by the Center for Medical Genetics, Ghent University Hospital, Ghent, Belgium. This study was approved by the Ethics Committee of Semmelweis University (SE RKEB no. 228/2018).

3.1.2 II. Study

25 patients (17 females and 8 males) with a mean age of 49 ± 13.8 years were included in the II. study where medical history was collected from the patients and NLM imaging was performed using skin biopsy samples.

During the enrollment process severity rating system was developed with semiquantitative methods taking into account the extent of calcium salts in the reticular dermis on the histopathological samples of 106 PXE patients. Five samples with the highest quality were chosen from each category of severity, resulting in a total of 25 samples.

All patients were diagnosed and managed at the PXE National Reference Center (MAGEC Nord), Angers University Hospital, Angers, France.

Patients were categorized in three groups based on the severity of the disease. We evaluated Phenodex score based on *Legrand et al.* and grouped the disease as mild (≤ 4), moderate (5-7) and severe (≥ 8) PXE [42].

Detailed medical history was collected from PXE patients including age, sex, onset and duration of the disease, smoking habit, skin symptoms (affected typical and nontypical skin sites), ophthalmological signs (CNV, AS, subretinal hemorrhage and scarring), cardiovascular phenotypes (blood pressure, electrocardiography (ECG), ABI), peripheral artery disease (PAD), presence of internal carotid artery hypoplasia (ICAH), degree of calcification of the aorta and peripheral vessels, history of angina pectoris, intermittent claudication, transitional

ischemic attack (TIA), stroke, gastrointestinal hemorrhage), presence of nephrolithiasis, osteopenia/osteoporosis and laboratory blood results.

All involved patients were informed about the study and signed the required consent (ethical approval number: SE RKEB 193-2/2017).

3.2 Multispectral LED-based device (MSI) and images analysis

We performed imaging using a multispectral LED prototype device at the Department of Dermatology, Venereology and Dermatooncology, Semmelweis University (Budapest, Hungary). This device has been previously detailed described [84,85].

The color CMOS 5-megapixel IDS camera (MT9P006STC, IDS uEye UI3581LE-C-HQ, Obersulm, Germany) of the device was fixed at 60 mm distance from the illuminated skin. Illumination was provided by an LED ring built into the device, which contained four different wavelengths of LED light (Figure 6/A, B). AF signal was excited using 405 nm LED illumination and registered in the green channel using a 515 nm high-pass filter. DR images were acquired using 660 and 940 nm illumination wavelengths (SML-LXL8047UVC, Lumex Inc., Ronkonkoma, NY, USA) (Figure 6/C). The LEDs have a field of view of 2×2 cm2 and an irradiation power density of 20 mW/cm2.

Seven different skin sites of each patient were analyzed by ImageJ v1.52a software (NIH, Bethesda, MD, USA) using the images acquired with 405 nm, 660 nm, 940 nm illumination wavelength settings.

We manually selected the regions of interests (ROI) based on their DS morphology according to patterns described earlier [65,66]. The selected ROI of AF images were transferred to DR images. The control group was provided by the uninvolved background skin. Images were analyzed using intensity descriptors in comparison to uninvolved skin. We analyzed the mean, minimum and maximum intensity values within the selected ROIs. Intensity values are expressed as arbitrary units (A.U.) as measured by ImageJ software.

Statistical analyses were performed with GraphPad Prism v9.0.0 software (GraphPad Software Inc., La Jolla, CA USA) using unpaired two-tailed Student's t-test. We considered p-values less than 0.05 statistically significant. All results are expressed as mean ± standard deviation.
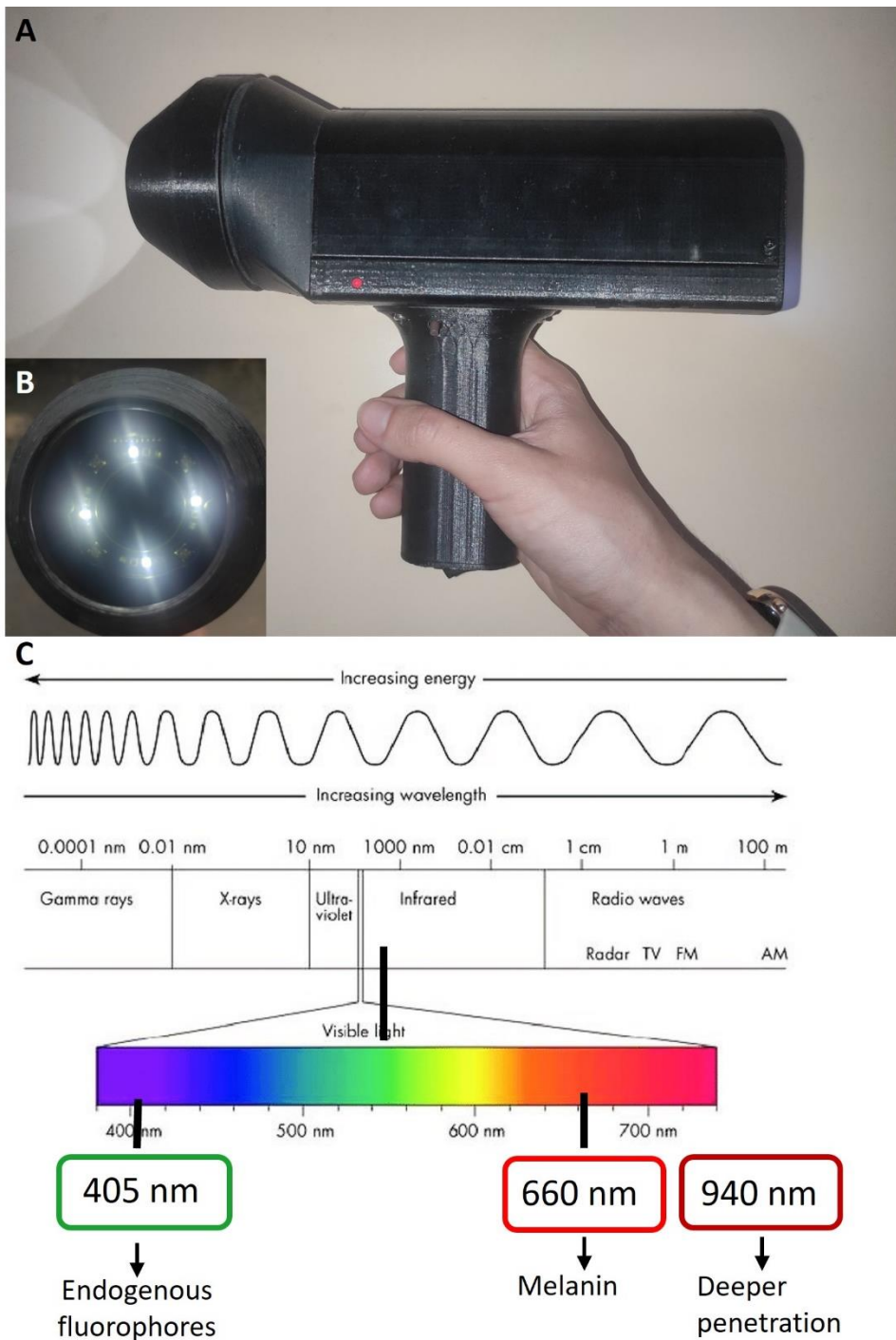
Figure 6. A) multispectral LED prototype device B) LED ring built into the device C) The utilized illumination wavelengths, and the main molecules which can be visualized [86].

3.3 Nonlinear microscopy (NLM)

From the same skin biopsy blocks 20 μm thick sections were cut and deparaffinized to visualize the skin structure under NLM. NLM imaging experiments were performed at the Nonlinear Microscopy Laboratory of Wigner Research Institute for Physics, Budapest, Hungary. NLM imaging was carried out using a ≈20 MHz repetition rate, sub-ps Ti:Sapphire laser (FemtoRose 300 TUN LC, R&D Ultrafast Lasers Ltd., Budapest, Hungary) working at 800 nm central wavelength with a bandwidth of <2 nm. A 20× water immersion objective (W-Plan – APOCHROMAT 20×/1.0 DIC (UV) VIS-IR, Carl Zeiss, Jena, Germany) was applied to focus the laser beam and a commercial Axio Examiner LSM 7 MP laser scanning two-photon microscope system (Carl Zeiss, Jena, Germany) with custom-modified detection optics was used to capture images. Two non-descanned detection (NDD) detectors collected the TPEF and SHG signals and signals were visualized by the ZEN 3.0 SR software (Carl Zeiss Microscopy GmbH, Jena, Germany). A 525/50 nm bandpass filter was used to collect TPEF signals of elastin and calcium deposits while 405/20 nm filter separated SHG signal of collagen. Mosaic images were captured from individual 2D imaging areas of 420 × 420 μm2. TPEF and SHG images were merged and compile into two-color mosaic images with ImageJ v1.46 software (NIH, Bethesda, MD, USA).

To determine the extent of calcification in patients, ten FOVs (field of view) were evaluated for each patient. Relative area affected by calcification (CA) (sum of the ROIs/total area of the ten FOVs) and calcification density (CD) (ratio of the above-threshold/total ROI area) were measured. Total calcification score (CS) was obtained by multiplying CD and CA.

CA, CD and CS values were compared between patients using Student's t-test or Mann-Whitney Wilcoxon exact test, as applicable. These values were compared to each parameter of Phenodex+ score, different levels of aortic calcification and peripheral atherosclerosis with the one-way ANOVA test.

The elastic fibers were measured manually using ImageJ software. The number of elastic fibers was given as the number of fibers divided by the FOV, and the length of fibers was given in μm units.

Pearson's correlation coefficient (r) or Spearman's correlation coefficient, where appropriate was used to explore the correlations between CA, CD, CS and the continuous variables. Logistic

regressions were built for dichotomous outcomes, while the Poisson regression models was utilized for analyzing count data. All the models were corrected for both age and gender.

4. Results

4.1 I. Study

In the I. study we found typical clinical presentations in all the enrolled PXE patients. Patients 2 and 5 showed moderate skin involvement, while in patients 1, 3 and 4 more extensive, prominent skin manifestations were detected (Figure 7).
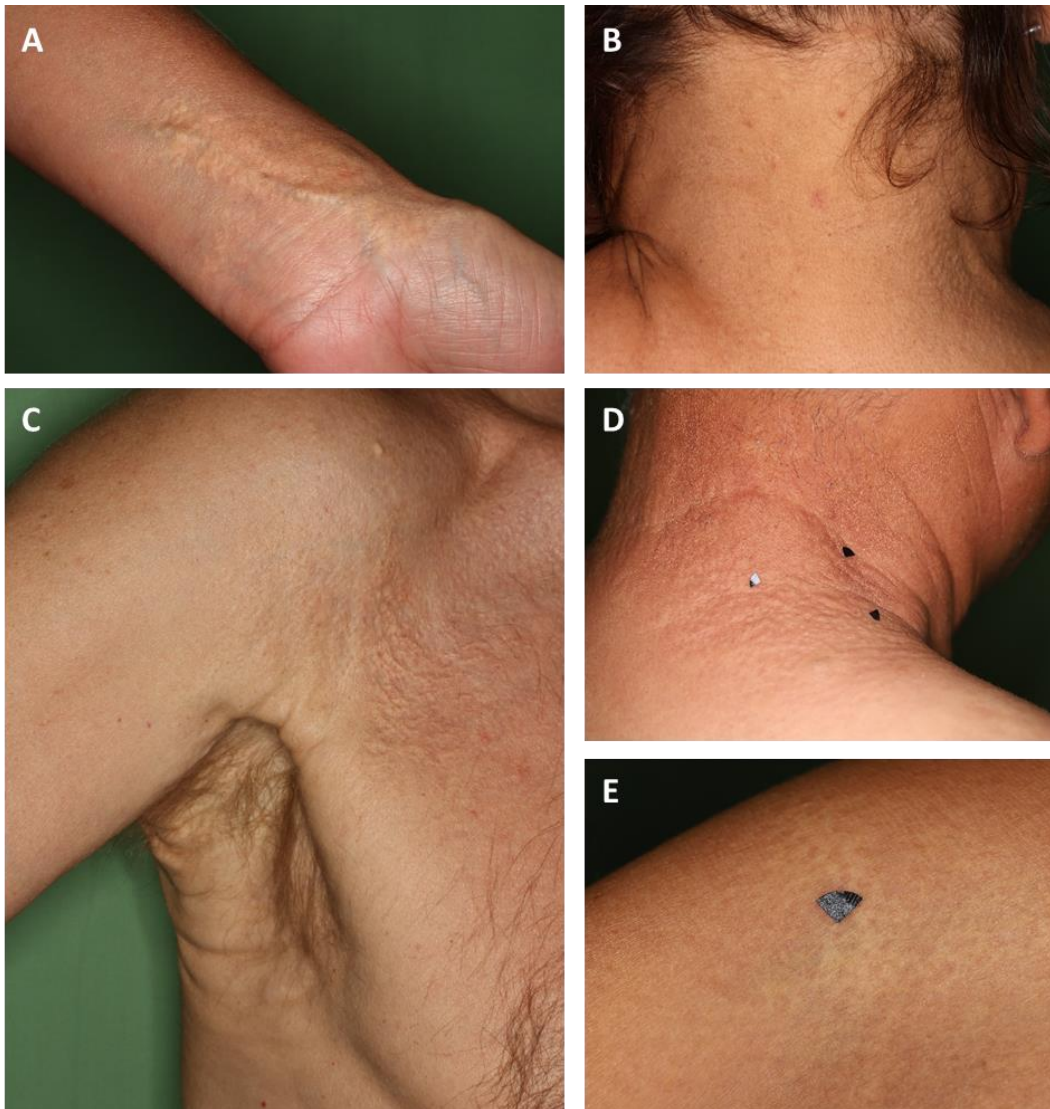

Figure 7. Clinical photographs that display the typical cutaneous manifestations of the patients with pseudoxanthoma elasticum. A) Patient 1, large coalescent plaques on the wrist B) Patient 2, 1–2 mm yellowish papules on the right side of the neck C) Patient 3, redundant, loose skin in the axilla and 2–5 mm papules on the axilla D) Patient 4, 2–6 mm papules on the right and dorsal side of the neck E) Patient 5, right antecubital fossa, yellow-white flat plaques. Black markers do not point to areas of interest, they are used for image alignment (area: 0.125 cm2).

While the neck was involved in all cases, yellowish papules on the periumbilical region were present in only two cases, and the chest was affected solely in Patient 1. A summary of the skin lesions' locations can be found in Table 3.

Table 3. Affected skin sites of the pseudoxanthoma elasticum patients.

Pt, patient; +, clearly visible papules or plaques; (+) mild, poorly visible skin lesions.

	Pt 1	Pt 2	Pt 3	Pt 4	Pt 5
neck	+	+	+	+	+
axilla	+	(+)	+	+	(+)
antecubital fossa	+	(+)	+	(+)	+
popliteal fossa	+	(+)	+	(+)	(+)
inguinal	+	+	+		(+)
periumbilical	+				+
wrist	+			(+)	
chest	(+)				

Characteristic histological features were noted under light microscopy using specific stains. Hematoxylin and eosin staining demonstrated a disordered arrangement of the connective tissue structure. Von Kossa staining revealed considerable calcium deposition in the mid-dermis. Weigert's elastic staining showed the fragmentation of mineralized elastin, and van Gieson staining revealed disrupted collagen fibers surrounding calcified regions (Figure 8).
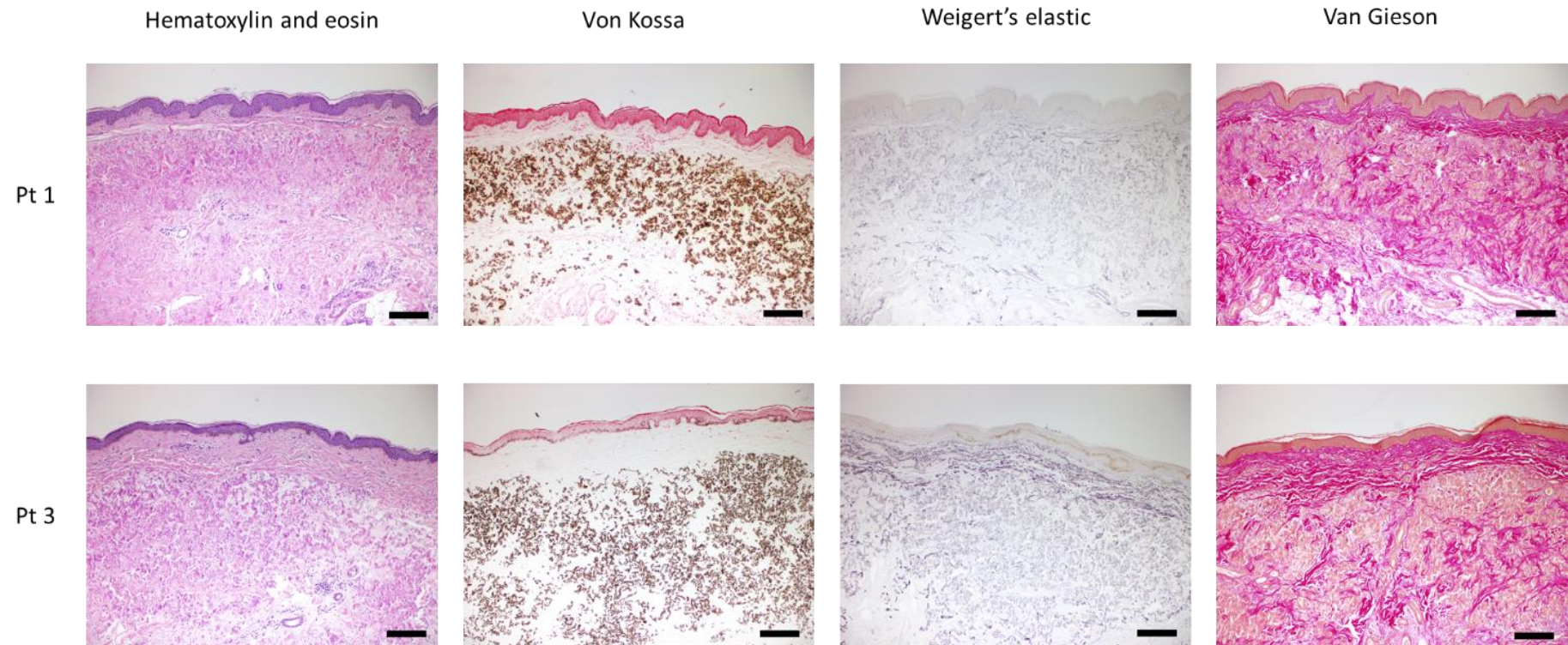
Figure 8. Histopathological characteristics of skin biopsies of the pseudoxanthoma elasticum patients (Pt) with hematoxylin and eosin (H&E), von Kossa (VK) staining for calcium deposits, Weigert's elastic (WE) staining for elastin and van Gieson (VG) staining for collagen. Scale bars display 100 μm. Representative images are shown at 100x magnification.

Yellowish clods on a light purplish-red background and reticulated vessels were typically observed in the acquired DS images. The globules presented as dots, irregular mesh networks, or parallel lines. However, in some of the clinically affected skin regions, these characteristic DS features were absent, as reported in Table 4.

Table 4. Characteristic dermoscopic features of the affected skin sites of the pseudoxanthoma elasticum patients according to the nomenclature of *Berthin et al.* [65] and *Kawashima et al.* [66].

Pt, patient. Blank cells indicate that DS images were not captured in that region, due to the lack of cutaneous manifestations.

	Structure	Pt 1	Pt 2	Pt 3	Pt 4	Pt 5
neck	globules	**plaques**	**dots, linear**	**mesh network**	**linear**	**dots, plaques**
	background	red	brownish	purple-red	red	brownish
	vessels	reticulated, linear	reticulated	reticulated	reticulated	no
axilla	globules	**plaques**	**dots**	**mesh network**	**dots**	**dots**
	background	purple	brownish	purple-red	pink	brownish
	vessels	linear	no	reticulated	no	no
antecubital fossa	globules	**linear**		**linear**	**linear**	**plaque**
	background	purple-red	**(non-typical)**	purple	brownish	purple
	vessels	reticulated		reticulated	no	no
popliteal fossa	globules	**linear**	**linear**	**linear**	**dots**	**linear**
	background	purple-red	brownish	purple	pink	purple
	vessels	several reticulated	no	reticulated	reticulated	reticulated
inguinal	globules	**dots**				
	background	purple	**(non-typical)**	**(non-typical)**		**(non-typical)**
	vessels	reticulated				
periumbilical	globules	**dots**				
	background	purple-red				**(absent)**
	vessels	reticulated				
wrist	globules	**plaques**				
	background	purple			**(absent)**	
	vessels	reticulated				
chest	globules					
	background	**(absent)**				
	vessels					

The skin lesions displayed a high-contrast signal in the AF images, even in skin areas where atypical or no DS patterns were detected (Figure 9).

Quantitative analyses revealed significantly higher mean AF intensity values in the PXE-affected skin areas compared to uninvolved skin (60.74 ± 23.86 vs. 43.40 ± 16.76 A.U.; $p < 0.0008$, (Figure 10/ A, B). We found significantly higher rates in the affected areas while measuring the minimum (36.14 ± 15.29 vs. 25.17 ± 11.66 A.U.; $p < 0.0012$) and the maximum values (109.8 ± 30.87 vs. 79.69 ± 23.76 A.U.; $p < 0.0001$) of AF intensity (Figure 10/B). Analyzing DR images with 660 and 940 nm illumination of the same field of views, no significant differences were found.
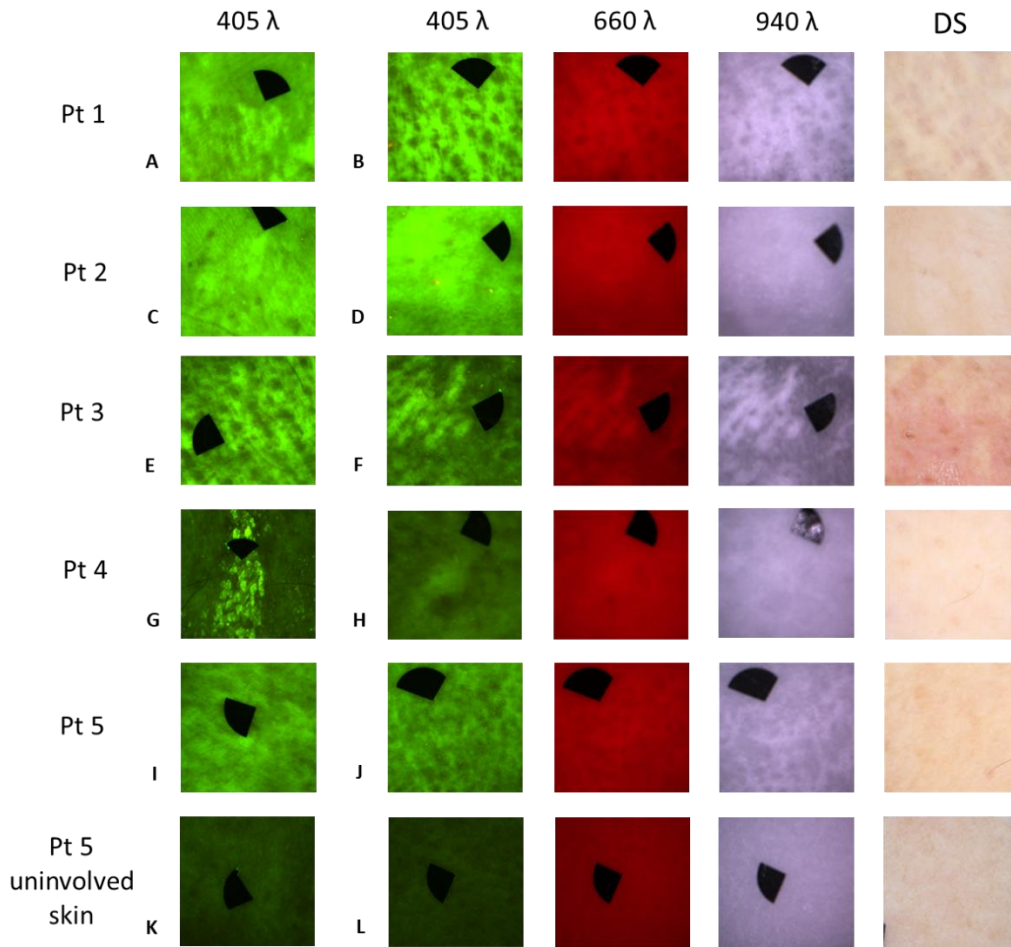
Figure 9. Representative autofluorescence (AF), diffuse reflectance (DR) and dermoscopy (DS) images of the affected skin sites of the pseudoxanthoma elasticum patients. **A**) AF image of the axilla of Patient (Pt) 1. **B**) AF, DR and DS images of the antecubital fossa of Pt 1, showing PXE-specific morphologic structures. **C**) AF image of the axilla of Pt 2. **D**) AF, DR and DS images of the inguinal region of Pt 2. AF image reveals a well-visible extensive area with high AF signal. DR images show barely noticeable pattern. DS image shows no typical pattern. **E**) AF image of the antecubital fossa of Pt 3. F) AF, DR and DS images of the neck of Pt 3, showing PXE-specific morphologic structures. **G**) AF image from popliteal fossa of Pt 4. **H**) AF, DR and DS images from wrist of Pt 4. AF image gives high-contrast signal. DR images are less informative. I) AF image of the inguinal region of Pt 5. **J**) AF, DR and DS images of the axilla of Pt 5, displaying PXE-specific morphologic structures. **K**) AF images of Pt 5, uninvolved normal skin. **L**) AF, DR and DS images of uninvolved normal skin, upper arm of Pt 5. The size of the images is 2×2 cm^2. Black markers do not point to areas of interest, they are used for image alignment (area: 0.125 cm^2).
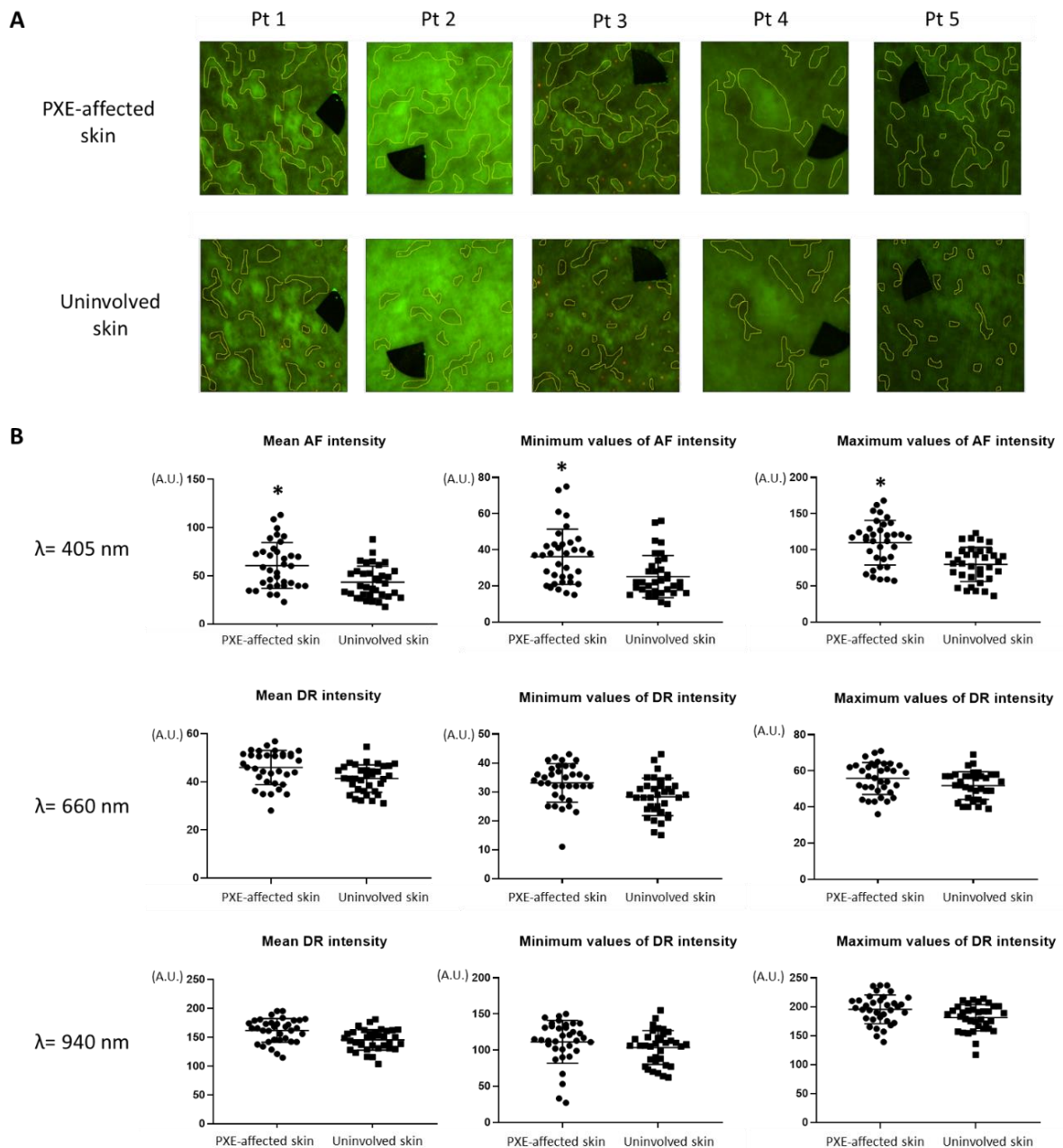
Figure 10. Regions of interest (ROI) selection and results of quantitative analyses of autofluorescence (AF) and diffuse reflectance (DR) images of the skin of the pseudoxanthoma elasticum (PXE) patients. A) Marked PXE-affected and uninvolved skin areas as ROI. Patient (Pt) 1, neck; Pt 2, antecubital fossa; Pt 3, axilla; Pt 4, wrist; Pt 5, antecubital fossa. B) In the AF images, the investigated parameters were significantly increased in PXE-affected skin compared to uninvolved skin. Analyzing DR images, no significant differences were found between PXE-affected and healthy skin. * $p < 0.05$. A.U., arbitrary unit.

4.2 II. Study

In the II. study, regarding the laboratory findings, a deficiency of vitamin K was observed in 4 individuals (16%), while hypercholesterolemia and high Lp(a) levels were detected in 9 patients (36%).

Table 5 shows a comparison of statistics results of the clinical variables and complications in PXE with data reported in the literature.

Table 5. PXE patient characteristics.

Data is expressed as mean ± standard error for normally distributed continuous variables, median for non-parametric distributed continuous variables and number (%) for categorical variables.

Abbreviations: CA: calcification area, CD: calcification density, CS: total calcification score, ICAH: internal carotid artery hypoplasia, TIA: transient ischemic attack, ECG: electrocardiography

	In this study cohort	Data from the literature
Total (n)	25	
Age (years)	48.4 ± 13.87	31.7 [87], 47±15 [40]
Male sex (n)	8 (32%)	32% [41], 36% [40]
Onset (age[years])	20 [14-22.5]	13.54 [88] 21±14 [89]
Duration (years)	20.5 ± 15.8	
Smoking (n)	10 (40%)	35% [88], 30% [40]
BMI (kg/cm^2)	24.27 (22.93–18.10)	
Osteopenia/osteoporosis (n)	6 (24%)	23-46% [40]
Gastrointestinal haemorrhage (n)	1 (4%)	18% [87]
Nephrolithiasis (n)	6 (24%)	39.8% [90]
Skin (n)		
Plaques	15 (60%)	
Redundant skin folds	7 (28%)	93% [87]
Acneiform lesions	10 (40%)	
Mucosal involvement	10 (40%)	21.4% [91]
Typical areas	6.2 ± 1.8	
Atypical areas	0 [0-1]	
CA	23.3 ± 16.15	
CD	51.6 ± 22.1	
CS	1436.0 ± 1182.5	
Elastic fiber number/FOV	40.8 ± 27.7	
Elastic fiber length (μm)	32.3 [25.4-34.9]	

Eye (n)		
Peau d'orange	4 (16%)	84.9% [89]
Angioid streaks	22 (88%)	93.75% [92], 92.5% [89]
Choroidal neovascularization	10 (40%)	42.5% [92], 50.9% [89]
Bleeding and/or scarring	2 (8%)	44% [89]
Macular atrophy	5 (20%)	32% [93]
Blindness	5 (20%)	10.9% [94]
Vascular (n)		
Weak or absent pulses	7 (28%)	
Intermittent claudication	9 (36%)	42-53% [95]
Lower limb revascularization	0 (0%)	
ICAH	4 (16%)	8.6% [96]
Peripheral artery disease	7 (28%)	37-57% [97]
High blood pressure	4 (16%)	8-25% [95]
Stroke/TIA	1 (4%)	15% [56]
Ankle-brachial index	1.1 [0.83-1.15]	0.92±0.19% [97]
Cardiac (n)		
Chest pain/ angina /abnormal ECG	5 (20%)	13-15% [56]
Cardiac attack	0 (0%)	1-5% [56]
Phenodex+ score	5.64 ± 1.8	
S	2 [1-2.5]	
E	2 [2-3]	
GI	0 [0-0]	
V	1 [0-2]	
C	0 [0-0]	
R	0 [0-0.5]	

NLM showed different degrees of calcification in patient skin biopsy samples (Figure 11).
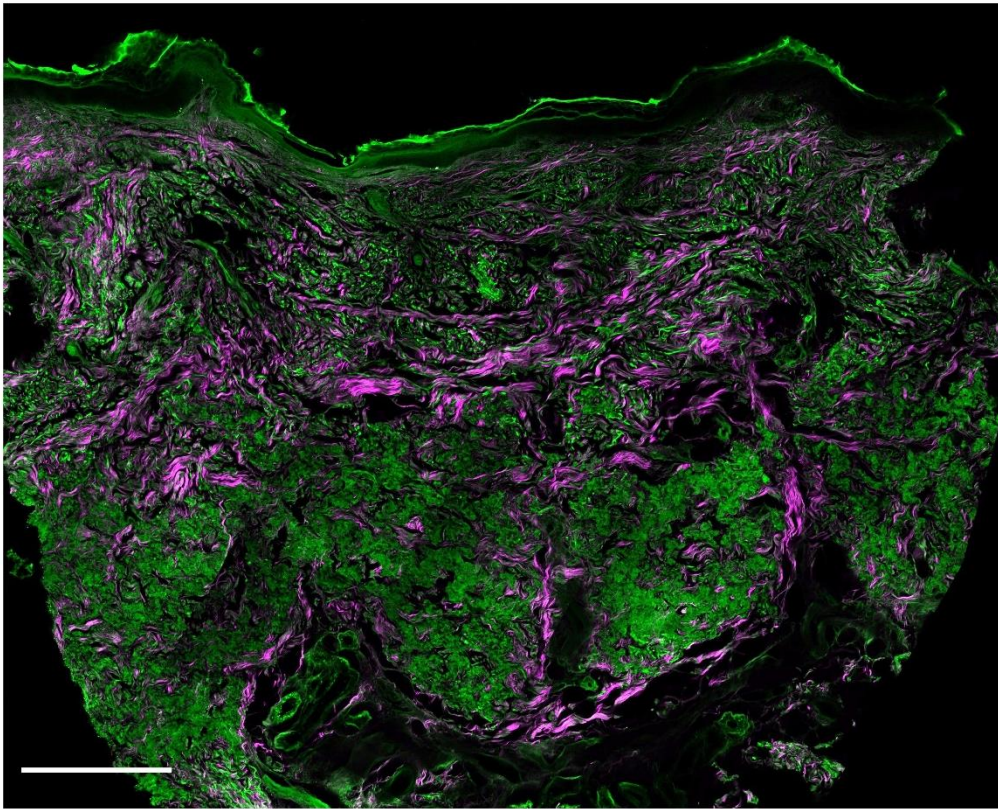
Figure 11. Nonlinear microscopic image of *ex vivo* formalin-fixed, deparaffinized, unstained PXE skin sections. Mosaic two-photon excitation fluorescence (TPEF) and second-harmonic generation (SHG) image of the skin sample of Patient 19. Scale bars display 400 μm.

Regarding the measurement of the extension of calcification, mean CA was 23.35±16.15 %, the median CD was 52.02 % (43.11–71.03), and CS was 1387 (264.9–1996).

In patients with severe Phenodex score, significantly higher CA, CD and CS were found than in the mild PXE patients (p=0.036; p=0.027; p=0.010). Moreover, significantly higher CS was observed in the severe vs moderate (p=0.041) Phenodex+ patients.

We found significantly higher CA values in patients with more severe ophthalmological complications (p=0.04) and with higher V-score (p=0.005) and with redundant skin folds (p=0.024). CA correlated significantly with the extent of vessel involvement (V-score) (r=0.434), peripheral atherosclerosis (r=0.44), the Phenodex+ score (r=0.435), the number of affected skin sites (r=0.48), and disease duration (r=0.48). The presence of macular atrophy (β=-0.44, p=0.032), acneiform changes (β=0.40, p=0.047) and late onset disease (β=-0.48, p=0.017) showed statistically significant associations with higher CA.

Significantly higher CD was found in patients with higher V-score (p=0.018), and with internal carotid artery hypoplasia (ICAH) (p=0.045). CD correlated significantly with V-score (r=0.539), peripheral atherosclerosis (r=0.0.41), and with the Phenodex+ score (r=0.46).

Higher CS was found in patients with acneiform skin lesions. CS correlated significantly with V-score (r=0.507), peripheral atherosclerosis (r=0.45), the Phenodex+ score (r=0.503), number of affected typical skin sites (r=0.49), and disease duration (r=0.40).

The number of affected typical skin was significantly higher in patients with CNV (p=0.033), redundant skin folds (p<0.0001), with higher S-score (p<0.0001) and significantly correlated with the Phenodex+ score (r=0.56, p=0.003).

Patients with affected nontypical skin sites had a higher occurrence of CNV (pOR 5.02, 95% CI [1.33 – 2225.12], p=0.02).

The main findings are summarized in Table 6 and Figure 12.

Table 6. Relationship between skin calcification parameters and clinical variables

Spearman's rho is presented for significant relationships in bold. Non-significant associations are marked as NS.

Abbreviations: ABI: ankle-brachial index, C: cardiac, CA: calcification area, CD: calcification density, CS: total calcification score, E: eye, GI: gastrointestinal, R: renal, S: skin, V: vessel

	CA	CD	CS
CD	**0.67**	**1**	NS
Elastic fiber number	**-0.74**	NS	NS
Elastic fiber length	**-0.42**	NS	**-0.586**
Onset	NS	NS	NS
Duration	**0.48**	NS	**0.40**
Visus	NS	NS	NS
ABI	NS	NS	NS
Aortic calcification	**-0.44**	NS	NS
Peripheral atherosclerosis	**0.44**	**0.41**	**0.45**
Number of affected typical skin sites	**0.48**	NS	**0.49**
Phenodex+ score	**0.435**	**0.46**	**0.503**
S-score	NS	NS	NS
E-score	NS	NS	NS
GI-score	NS	NS	NS
C-score	NS	NS	NS
V-score	**0.434**	**0.539**	**0.507**
R-score	NS	NS	NS
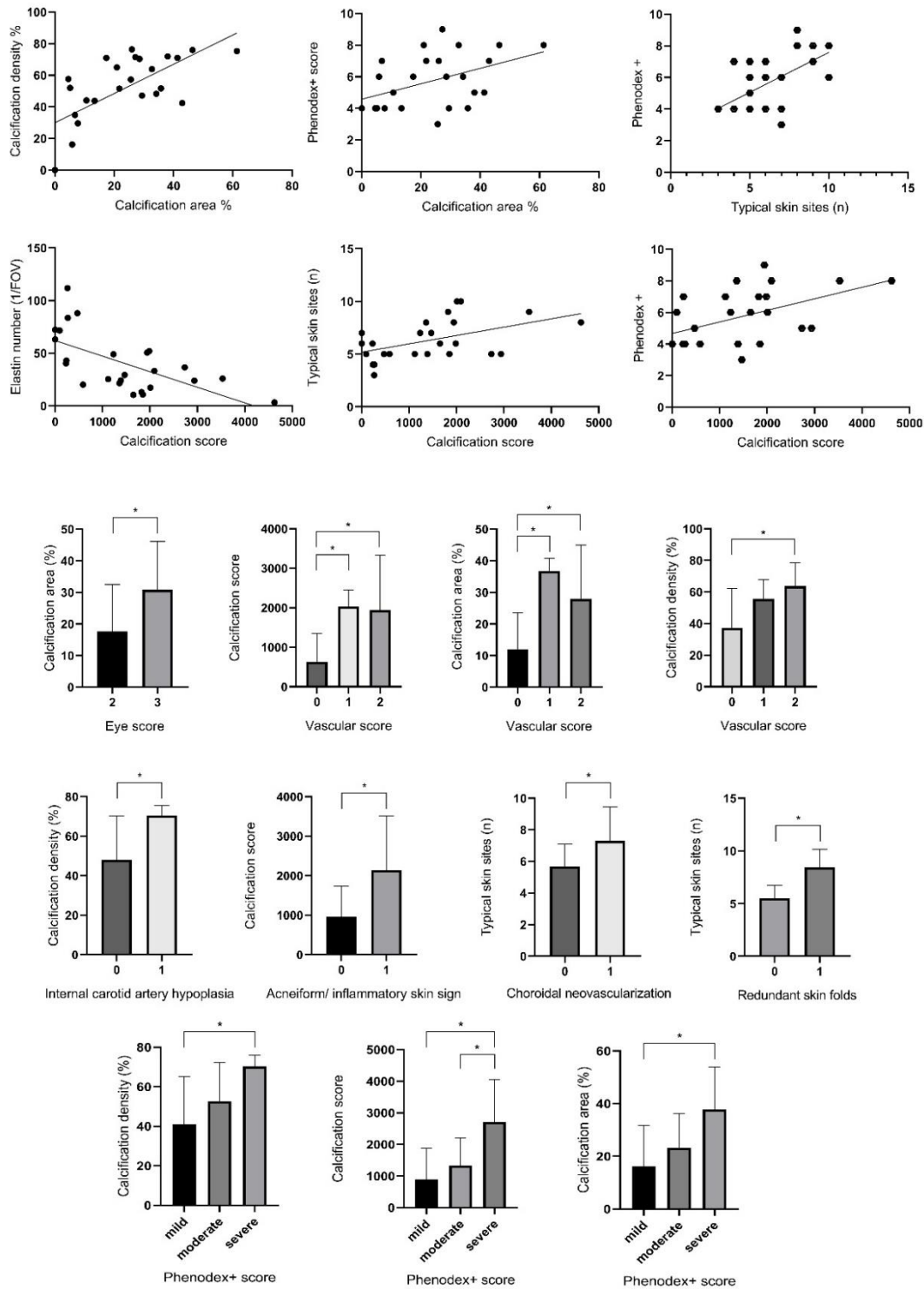
Figure 12. Association between skin calcification parameters and macroscopic skin signs or clinical

phenotypes in the investigated pseudoxanthoma elasticum patients. Statistical significance (p<0.05) is marked with *.

5. Discussion

Modern imaging techniques have made remarkable progress in numerous medical fields and have been integrated into routine clinical practice [98].

Skin imaging is valuable not only because the skin is the most easily accessible organ, but also because the different morphological variations of the skin are crucial in the differential diagnosis of various conditions. Several different imaging tools can be used to examine the skin, however, most of these have not been widely used in clinical practice yet [99].

In this work, we introduced two different novel skin imaging methods and showed their use and importance in PXE. We attempted to visualize PXE-affected skin sites and evaluate them objectively.

DS – also known as the dermatologist's s stethoscope – gains an essential role in clinical practice, as a characteristic pattern is described in an increasing number of skin diseases. It is easily available and frequently used everyday tool in dermatological practice [100]. With MSI, we were able to effectively visualize skin regions affected by PXE, including those where DS failed to reveal PXE-specific structures. Under different wavelengths, varying degrees of intensity of PXE lesions was observed. In some cases, it was not feasible to differentiate the PXE-affected skin using DR images and were generally less informative compared to AF images and did not appear to offer a notable advantage over DS. AF images exhibited significantly higher intensity, making the affected areas clearly visible.

Both DS and MSI are non-invasive, fast, cost-effective and portable imaging tools. However, with the use of MSI, we were able to visualize PXE lesions with higher contrast and select the affected areas more precisely, thus allows quantification of the severity of skin involvement.

We suppose that the higher AF intensity in PXE-affected skin lesions is associated with the absorption of light by calcium deposits, which are primarily composed of calcium hydrogen phosphate and calcium hydroxyapatite, and in some extent of iron precipitates [101,102]. It was reported that calcium hydroxyapatite in nanoparticle has fluorescence properties, with maximum excitation intensity at 405 nm [103]. Since we used the same illumination wavelength, we hypothesize that AF signal originates from calcium hydroxyapatite in the skin. Additionally, fluorescence microscopy has demonstrated that calcium phosphate emits AF at 345 and 470 nm

excitation wavelength, indicating that calcium phosphate may also produce an AF signal when illuminated at 405 nm [104].

Further research would be required to explore the precise source of the increased AF signal observed in PXE lesions under 405 nm excitation [105]. However, determining the optimal LED illumination wavelength for AF could potentially enhance the specificity of imaging for PXE skin lesions.

The extent of skin calcification and the disruption of elastic fibers were quantitative analyzed using NLM images, for the objective assessment of the severity of the skin lesions. Therefore, we could compare the severity of the skin manifestation with the systemic involvements and correlate it with several different parameters.

According to a recent retrospective clinical study of 125 PXE patients, there should be a link between the severity of cardiovascular and ophthalmological complications and the number of PXE affected skin sites [41]. *Utani et al.* reported associations between higher number of PXE affected skin sites and cardiovascular disease, and wider angioid streaks [91]. Similarly as seen in previous studies, we found that the number of affected typical or nontypical skin sites was significantly higher in patients with CNV.

In our study, all investigated calcification indexes were significantly higher in patients with high Phenodex+ scores. In recent studies, where the 18F-Sodium Fluoride (18F-NaF) uptake in the skin showed the active calcification in PXE, higher 18F-NaF deposition was detected in the neck of patients with higher Phenodex scores. However, 18F-NaF accumulation in the arteries or other skin sites did not show any significant correlation with Phenodex score [50,106].

It has been previously studied that metabolic abnormalities in PXE predisposes to early initiation and accelerated occurrence of age-related vascular process [57]. PAD is highly increased in PXE [56,95,107,108]. In our study CA, CD, CS was significantly correlated with V-score and with peripheral atherosclerosis, which results suggest an association between the severity of skin symptoms and the development of vascular manifestations.

Before adjustment, significantly higher CD was found in patients with weak pulses (p=0.016) and with intermittent claudication (p=0.041) and higher CS was significantly higher in patients with weak pulses (p=0.028). This may be due to the correlation with age described in a recent study, which showed that disease severity and arterial calcification were strongly dependent on age in PXE [109].

We suppose that negative correlation between CA and number of elastic fibers is due to the higher calcification masking the elastic fibers. The reason for the negative correlation between CA, CS, and the length of elastic fibers is that calcification leads to fragmentation of the elastic fibers.

The two introduced techniques (MSI and NLM) are not yet widely accessible to clinicians.

The limitation of the MSI device is its field of view, which covers only 2×2 cm^2, which restricts the maximum area that can be captured. This device did not have tunable wavelength, so accordingly, we could not select the most optimal LED illumination wavelength for the assessment of PXE- affected area and the different AF molecules cannot be displayed separately.

NLM was utilized *ex vivo*, and the samples preparation, image acquisition, and image processing are all time-consuming procedures.

The analysis of the captured images was carried out manually which also required substantial amount of time and may not be entirely exact. Subsequently, our future plans involve the implementation of automatic image analysis.

Other non-invasive techniques that can be used to visualize PXE lesions also have significant limitations. Both HFUS, OCT and RCM are expensive methods that demand expertise and specialized training, and they are found only at larger dermatology centers [67-69].

These modalities, utilized in our research, could also have potential benefits in other connective tissue disorders and cutaneous calcinosis [33,34].

6. Conclusions

I.   Study

I/ 1. In our study, we evaluated *in vivo* visualization of the characteristic skin changes in PXE.

I/ 2. We utilized *in vivo* MSI device on the skin of PXE patients to visualize the characteristic dermoscopic features.

I/ 3. We found that characteristic dermoscopic features appeared in high contrast using 405 nm illumination (autofluorescence light), where we have successfully separated PXE-affected and healthy skin areas.

I/ 4. Quantitative analyses revealed significantly higher mean AF intensity, significantly higher minimum and maximum AF values in the PXE-affected skin areas compared to uninvolved skin.

II.   Study

II/ 1. We explored association between the extension of the skin manifestations and the severity of the systemic involvement.

II/ 2. We evaluated the skin involvement objectively and quantitatively.

II/ 3. We assessed the skin severity by the extent of ectopic calcification in the skin using *ex vivo* NLM.

II/ 4. We created parameters which can be used to determine the amount of skin calcification (calcified area, CA; calcification density, CD; total calcification score, CS).

II/ 5. Quantitative analyses were carried out; Associations were observed between the investigated parameters and clinical manifestations:

- CA showed significant correlation with the number of affected typical skin sites, the Phenodex+ score, peripheral atherosclerosis, extent of vessel involvement (V-score) and disease duration and showed significant association with the presence of macular atrophy, acneiform skin lesions and late onset disease. Patients with more severe eye and vascular complications had significantly higher CA.

- CD correlated significantly with V-score and it was significantly higher in patients with internal carotid artery hypoplasia.

- Significantly higher CS was observed in the severe vs moderate (p=0.041) Phenodex+ patients. Higher CS was found in patients with acneiform skin lesions and CS correlated

significantly with V-score, peripheral atherosclerosis, the Phenodex+ score, number of affected typical skin sites, and disease duration.

- Significantly higher CA, CD and CS were found in patients with severe Phenodex score than in the mild PXE patients.

7. Summary

Pseudoxanthoma elasticum (PXE) is a rare connective tissue disorder that can cause severe ocular and cardiovascular complications.

Novel imaging modalities have been used to investigate and quantify the severity of skin lesions and to reveal the relationship between skin calcification and systemic involvement in PXE patients.

In addition to dermoscopy, we introduced a novel multispectral imaging (MSI) device and used autofluorescence (AF) and diffuse reflectance (DR) imaging techniques, to assess the affected skin sites of five PXE patients. Our results showed significantly higher AF intensity values in areas of PXE-affected skin when compared to uninvolved skin. This suggests that AF imaging can be used to observe skin lesions and objectively monitor the efficacy of novel therapeutic approaches in PXE patients. Furthermore, it is a safe, fast, and cost-effective method that can be applied conveniently.

Ex vivo nonlinear microscopy (NLM) imaging was utilized to assess the extent of skin calcification in 25 PXE patients. Two-photon absorption fluorescence (TPEF) method was used to acquire images for quantitative analyses of ectopic calcification and elastic fibers. After statistical analyses, a significant correlation was found between the calcified area (CA) and the number of affected typical skin sites, disease duration, and ophthalmological and cardiovascular complications. We also found a significant association between higher CA and the presence of macula atrophy and acneiform skin lesions. The findings suggest that NLM imaging may be useful for clinicians to identify PXE patients who are at risk of developing severe systemic complications.

The first sign of PXE often appears on the skin. Consequently, the diagnosis based on skin manifestations may prevent the development of systemic manifestations and slow down the progression of the disease with prompt, early management. The quantitative assessment of the skin lesions with MSI and NLM techniques may provide novel possibilities to monitor the severity of skin lesions, predict the development of systemic involvements and may be implemented into diagnostic approaches used in PXE in the future.

8. References

1. Jartarkar, S.R.; Patil, A.; Wollina, U.; Gold, M.H.; Stege, H.; Grabbe, S.; Goldust, M. New diagnostic and imaging technologies in dermatology. *J Cosmet Dermatol* **2021**, *20*, 3782-3787, doi:10.1111/jocd.14499.

2. Hibler, B.P.; Qi, Q.; Rossi, A.M. Current state of imaging in dermatology. *Semin Cutan Med Surg* **2016**, *35*, 2-8, doi:10.12788/j.sder.2016.001.

3. Schneider, S.L.; Kohli, I.; Hamzavi, I.H.; Council, M.L.; Rossi, A.M.; Ozog, D.M. Emerging imaging technologies in dermatology: Part I: Basic principles. *J Am Acad Dermatol* **2019**, *80*, 1114-1120, doi:10.1016/j.jaad.2018.11.042.

4. Welzel, J.; Schuh, S. Noninvasive diagnosis in dermatology. *J Dtsch Dermatol Ges* **2017**, *15*, 999-1016, doi:10.1111/ddg.13347.

5. Plázár, D.; Joura, M.I.; Kiss, N.; Medvecz, M. [Dermoscopy of genodermatoses]. *Dermatologie (Heidelb)* **2023**, *74*, 256-261, doi:10.1007/s00105-023-05124-7.

6. Chen, X.; Lu, Q.; Chen, C.; Jiang, G. Recent developments in dermoscopy for dermatology. *J Cosmet Dermatol* **2021**, *20*, 1611-1617, doi:10.1111/jocd.13846.

7. Wortsman, X.; Alfageme, F.; Roustan, G.; Arias-Santiago, S.; Martorell, A.; Catalano, O.; Scotto di Santolo, M.; Zarchi, K.; Bouer, M.; Gonzalez, C.; Bard, R.; Mandava, A.; Gaitini D. Guidelines for Performing Dermatologic Ultrasound Examinations by the DERMUS Group. *J Ultrasound Med* **2016**, *35*, 577-580, doi:10.7863/ultra.15.06046.

8. Csernus, A.E.; Lengyel, Z.; Ferencz, J.; Battyáni, I.; Kálmán, E.; Battyáni, Z. Melanoma malignum in vivo mélységi terjedésének meghatározása nagyfelbontású ultrahanggal (18-, 22 Mhz). *BŐRGYÓGYÁSZATI ÉS VENEROLÓGIAI SZEMLE* **2012**, *vol. 88, no. 1, pp. 11–18.*

9. Hernandez-Ibanez, C.; Blazquez-Sanchez, N.; Aguilar-Bernier, M.; Fúnez-Liébana, R.; Rivas-Ruiz, F.; de Troya-Martin, M. Usefulness of high-frequency ultrasound in the classification of histologic subtypes of primary basal cell carcinoma. *Actas Dermo-Sifiliográficas (English Edition)* **2017**, *108*, 42-51.

10. DeJong, H.M.; Abbott, S.; Zelesco, M.; Kennedy, B.F.; Ziman, M.R.; Wood, F.M. The validity and reliability of using ultrasound elastography to measure cutaneous stiffness, a systematic review. *Int J Burns Trauma* **2017**, *7*, 124-141.

11. Alfageme, F.; Wortsman, X.; Catalano, O.; Roustan, G.; Crisan, M.; Crisan, D.; Gaitini, D.E.; Cerezo, E.; Badea, R. European Federation of Societies for Ultrasound in

Medicine and Biology (EFSUMB) Position Statement on Dermatologic Ultrasound. *Ultraschall Med* **2021**, *42*, 39-47, doi:10.1055/a-1161-8872.

12. Welzel, J.; Lankenau, E.; Birngruber, R.; Engelhardt, R. Optical coherence tomography of the human skin. *Journal of the American Academy of Dermatology* **1997**, *37*, 958-963.

13. Rajabi-Estarabadi, A.; Bittar, J.M.; Zheng, C.; Nascimento, V.; Camacho, I.; Feun, L.G.; Nasiriavanaki, M.; Kunz, M.; Nouri, K. Optical coherence tomography imaging of melanoma skin cancer. *Lasers Med Sci* **2019**, *34*, 411-420, doi:10.1007/s10103-018-2696-1.

14. De Carvalho, N.; Schuh, S.; Kindermann, N.; Kästle, R.; Holmes, J.; Welzel, J. Optical coherence tomography for margin definition of basal cell carcinoma before micrographic surgery-recommendations regarding the marking and scanning technique. *Skin Res Technol* **2018**, *24*, 145-151, doi:10.1111/srt.12407.

15. Psomadakis, C.E.; Marghoob, N.; Bleicher, B.; Markowitz, O. Optical coherence tomography. *Clin Dermatol* **2021**, *39*, 624-634, doi:10.1016/j.clindermatol.2021.03.008.

16. Rajabi-Estarabadi, A.; Vasquez-Herrera, N.; Martinez-Velasco, M.; Tsatalis, J.; Verne, S.; Nouri, K.; Tosti, A. Optical coherence tomography in diagnosis of inflammatory scalp disorders. *Journal of the European Academy of Dermatology and Venereology* **2020**, *34*, 2147-2151.

17. Rajadhyaksha, M.; Marghoob, A.; Rossi, A.; Halpern, A.C.; Nehal, K.S. Reflectance confocal microscopy of skin in vivo: From bench to bedside. *Lasers in surgery and medicine* **2017**, *49*, 7-19, doi:10.1002/lsm.22600.

18. Nwaneshiudu, A.; Kuschal, C.; Sakamoto, F.H.; Anderson, R.R.; Schwarzenberger, K.; Young, R.C. Introduction to confocal microscopy. *The Journal of investigative dermatology* **2012**, *132*, e3, doi:10.1038/jid.2012.429.

19. Gust, C.; Schuh, S.; Welzel, J.; Daxenberger, F.; Hartmann, D.; French, L.E.; Ruini, C.; Sattler, E.C. Line-Field Confocal Optical Coherence Tomography Increases the Diagnostic Accuracy and Confidence for Basal Cell Carcinoma in Equivocal Lesions: A Prospective Study. *Cancers (Basel)* **2022**, *14*, doi:10.3390/cancers14041082.

20. Ustione, A.; Piston, D.W. A simple introduction to multiphoton microscopy. *J Microsc* **2011**, *243*, 221-226, doi:10.1111/j.1365-2818.2011.03532.x.

21.   Yue, S.; Slipchenko, M.N.; Cheng, J.X. Multimodal Nonlinear Optical Microscopy. *Laser Photon Rev* **2011**, *5*, doi:10.1002/lpor.201000027.

22.   Hoover, E.E.; Squier, J.A. Advances in multiphoton microscopy technology. *Nat Photonics* **2013**, *7*, 93-101, doi:10.1038/nphoton.2012.361.

23.   Helmchen, F.; Denk, W. Deep tissue two-photon microscopy. *Nat Methods* **2005**, *2*, 932-940, doi:10.1038/nmeth818.

24.   Hanson, K.M.; Bardeen, C.J. Application of nonlinear optical microscopy for imaging skin. *Photochem Photobiol* **2009**, *85*, 33-44, doi:10.1111/j.1751-1097.2008.00508.x.

25.   Tong, L.; Cheng, J.-X. Label-free imaging through nonlinear optical signals. *Materials Today* **2011**, *14*, 264-273, doi:https://doi.org/10.1016/S1369-7021(11)70141-9.

26.   Keikhosravi, A.; Bredfeldt, J.S.; Sagar, A.K.; Eliceiri, K.W. Second-harmonic generation imaging of cancer. *Methods Cell Biol* **2014**, *123*, 531-546, doi:10.1016/b978-0-12-420138-5.00028-8.

27.   Haluszka, D.; Lőrincz, K.; Molnár, G.; Tamás, G.; Kolonics, A.; Szipőcs, R.; Kárpáti, S.; Wikonkál, N.M. In vivo second-harmonic generation and ex vivo coherent anti-stokes raman scattering microscopy to study the effect of obesity to fibroblast cell function using an Yb-fiber laser-based CARS extension unit. *Microsc Res Tech* **2015**, *78*, 823-830, doi:10.1002/jemt.22545.

28.   Haluszka, D.; Lőrincz, K.; Kiss, N.; Szipőcs, R.; Kuroli, E.; Gyöngyösi, N.; Wikonkál, N.M. Diet-induced obesity skin changes monitored by in vivo SHG and ex vivo CARS microscopy. *Biomed Opt Express* **2016**, *7*, 4480-4489, doi:10.1364/boe.7.004480.

29.   Lőrincz, K.; Haluszka, D.; Kiss, N.; Gyöngyösi, N.; Bánvölgyi, A.; Szipőcs, R.; Wikonkál, N.M. Voluntary exercise improves murine dermal connective tissue status in high-fat diet-induced obesity. *Archives of dermatological research* **2017**, *309*, 209-215, doi:10.1007/s00403-017-1715-6.

30.   Cicchi, R.; Sestini, S.; De Giorgi, V.; Massi, D.; Lotti, T.; Pavone, F.S. Nonlinear laser imaging of skin lesions. *J Biophotonics* **2008**, *1*, 62-73, doi:10.1002/jbio.200710003.

31.   Kiss, N.; Krolopp, Á.; Lőrincz, K.; Bánvölgyi, A.; Szipőcs, R.; Wikonkál, N.M. Stain-free Histopathology of Basal Cell Carcinoma by Dual Vibration Resonance Frequency CARS Microscopy. *Pathol Oncol Res* **2018**, *24*, 927-930, doi:10.1007/s12253-017-0356-6.

32.   Anker, P.; Fésűs, L.; Kiss, N.; Lengyel, A.; Pinti, É.; Lihacova, I.; Lihachev, A.; Plorina, E.V.; Fekete, G.; Medvecz, M. A Cross-Sectional Study of the Dermatological

Manifestations of Patients with Fabry Disease and the Assessment of Angiokeratomas with Multimodal Imaging. *Diagnostics (Basel)* **2023**, *13*, doi:10.3390/diagnostics13142368.

33. Anker, P.; Fésűs, L.; Kiss, N.; Noll, J.; Becker, K.; Kuroli, E.; Mayer, B.; Bozsányi, S.; Lőrincz, K.; Lihacova, I.; Lihachev, A; Lange, M.; Wikonkál, N.M.; Medvecz, M. Visualization of Keratin with Diffuse Reflectance and Autofluorescence Imaging and Nonlinear Optical Microscopy in a Rare Keratinopathic Ichthyosis. *Sensors (Basel)* **2021**, *21*, doi:10.3390/s21041105.

34. Kiss, N.; Haluszka, D.; Lőrincz, K.; Kuroli, E.; Hársing, J.; Mayer, B.; Kárpáti, S.; Fekete, G.; Szipőcs, R.; Wikonkál, N.M.; Medvecz, M. Ex vivo nonlinear microscopy imaging of Ehlers-Danlos syndrome-affected skin. *Archives of dermatological research* **2018**, *310*, 463-473, doi:10.1007/s00403-018-1835-7.

35. Kiss, N.; Fésűs, L.; Bozsányi, S.; Szeri, F.; Van Gils, M.; Szabó, V.; Nagy, A.I.; Hidvégi, B.; Szipőcs, R.; Martin, L., Vanakker, O.; Arányi, T.; Merkely, B.; Wikonkál, N.M.; Medvecz, M. Nonlinear optical microscopy is a novel tool for the analysis of cutaneous alterations in pseudoxanthoma elasticum. *Lasers Med Sci* **2020**, *35*, 1821-1830, doi:10.1007/s10103-020-03027-w.

36. Rigal, D. Observations pour servir á l'histoire de la cheloide diffuse xantholasmique. *Ann Dermatol Syphiligr* **1881**, *2*, 491-495.

37. Darier, J. Pseudoxanthoma elasticum. *Monatsschr Prakt Dermatol* **1896**, *23*, 609-616.

38. Grönblad, E. Angioid streaks—Pseudoxanthoma elasticum: vorläufige mitteilung. *Acta Ophthalmologica* **1929**, *7*, 329-329.

39. Stranberg, J. Pseudoxanthoma elasticum. *Zbl Haut Geschlechtskr* **1929**, *31*, 689.

40. Martin, L.; Hoppé, E.; Kauffenstein, G.; Omarjee, L.; Navasiolava, N.; Henni, S.; Willoteaux, S.; Leftheriotis, G. Early arterial calcification does not correlate with bone loss in pseudoxanthoma elasticum. *Bone* **2017**, *103*, 88-92, doi:10.1016/j.bone.2017.06.017.

41. Navasiolava, N.; Gnanou, M.; Douillard, M.; Saulnier, P.; Aranyi, T.; Ebran, J.M.; Henni, S.; Humeau, H.; Leftheriotis, G.; Martin, L. The extent of pseudoxanthoma elasticum skin changes is related to cardiovascular complications and visual loss: a cross-sectional study. *Br J Dermatol* **2019**, *180*, 207-208, doi:10.1111/bjd.17094.

42. Legrand, A.; Cornez, L.; Samkari, W.; Mazzella, J.M.; Venisse, A.; Boccio, V.; Auribault, K.; Keren, B.; Benistan, K.; Germain, D.P.; Frank, M.; Jeunemaitre, X.;

Albuisson, J. Mutation spectrum in the ABCC6 gene and genotype-phenotype correlations in a French cohort with pseudoxanthoma elasticum. *Genet Med* **2017**, *19*, 909-917, doi:10.1038/gim.2016.213.

43. Bergen, A.A.; Plomp, A.S.; Schuurman, E.J.; Terry, S.; Breuning, M.; Dauwerse, H.; Swart, J.; Kool, M.; van Soest, S.; Baas, F.; ten Brink, JB.; de Jong, PT. Mutations in ABCC6 cause pseudoxanthoma elasticum. *Nat Genet* **2000**, *25*, 228-231, doi:10.1038/76109.

44. Szeri, F.; Miko, A.; Navasiolava, N.; Kaposi, A.; Verschuere, S.; Molnar, B.; Li, Q.; Terry, S.F.; Boraldi, F.; Uitto, J.; van de Wetering, K.; Martin, L.; Quaglino, D.; Vanakker, OM.; Tory, K.; Aranyi; T. The pathogenic c.1171A>G (p.Arg391Gly) and c.2359G>A (p.Val787Ile) ABCC6 variants display incomplete penetrance causing pseudoxanthoma elasticum in a subset of individuals. *Hum Mutat* **2022**, *43*, 1872-1881, doi:10.1002/humu.24498.

45. Köblös, G.; Andrikovics, H.; Prohászka, Z.; Tordai, A.; Váradi, A.; Arányi, T. The R1141X loss-of-function mutation of the ABCC6 gene is a strong genetic risk factor for coronary artery disease. *Genet Test Mol Biomarkers* **2010**, *14*, 75-78, doi:10.1089/gtmb.2009.0094.

46. Katona, E.; Aslanidis, C.; Remenyik, E.; Csikós, M.; Kárpáti, S.; Paragh, G.; Schmitz, G. Identification of a novel deletion in the ABCC6 gene leading to Pseudoxanthoma elasticum. *J Dermatol Sci* **2005**, *40*, 115-121, doi:10.1016/j.jdermsci.2005.07.010.

47. Favre, G.; Laurain, A.; Aranyi, T.; Szeri, F.; Fulop, K.; Le Saux, O.; Duranton, C.; Kauffenstein, G.; Martin, L.; Lefthériotis, G. The ABCC6 Transporter: A New Player in Biomineralization. *Int J Mol Sci* **2017**, *18*, doi:10.3390/ijms18091941.

48. Li, Q.; Arányi, T.; Váradi, A.; Terry, S.F.; Uitto, J. Research Progress in Pseudoxanthoma Elasticum and Related Ectopic Mineralization Disorders. *J Invest Dermatol* **2016**, *136*, 550-556, doi:10.1016/j.jid.2015.10.065.

49. Van Gils, M.; Nollet, L.; Verly, E.; Deianova, N.; Vanakker, O.M. Cellular signaling in pseudoxanthoma elasticum: an update. *Cell Signal* **2019**, *55*, 119-129, doi:10.1016/j.cellsig.2018.12.009.

50. Omarjee, L.; Mention, P.-J.; Janin, A.; Kauffenstein, G.; Pabic, E.L.; Meilhac, O.; Blanchard, S.; Navasiolava, N.; Leftheriotis, G.; Couturier, O.; Jeannin, P.; Lacoeuille, F.; Martin, L. Assessment of Inflammation and Calcification in Pseudoxanthoma Elasticum Arteries and Skin with 18F-FluroDeoxyGlucose and 18F-Sodium Fluoride

Positron Emission Tomography/Computed Tomography Imaging: The GOCAPXE Trial. *Journal of clinical medicine* **2020**, *9*, 3448, doi:10.3390/jcm9113448.

51.   Luo, H.; Faghankhani, M.; Cao, Y.; Uitto, J.; Li, Q. Molecular Genetics and Modifier Genes in Pseudoxanthoma Elasticum, a Heritable Multisystem Ectopic Mineralization Disorder. *Journal of Investigative Dermatology* **2021**, *141*, 1148-1156, doi:https://doi.org/10.1016/j.jid.2020.10.013.

52.   Gliem, M.; Zaeytijd, J.D.; Finger, R.P.; Holz, F.G.; Leroy, B.P.; Charbel Issa, P. An update on the ocular phenotype in patients with pseudoxanthoma elasticum. *Front Genet* **2013**, *4*, 14, doi:10.3389/fgene.2013.00014.

53.   Ellabban, A.A.; Hangai, M.; Yamashiro, K.; Nakagawa, S.; Tsujikawa, A.; Yoshimura, N. Tomographic fundus features in pseudoxanthoma elasticum: comparison with neovascular age-related macular degeneration in Japanese patients. *Eye (Lond)* **2012**, *26*, 1086-1094, doi:10.1038/eye.2012.101.

54.   Nolte, K.B. Sudden cardiac death owing to pseudoxanthoma elasticum: a case report. In *Hum Pathol*, United States, 2000; Vol. 31, pp. 1002-1004.

55.   Kornet, L.; Bergen, A.A.; Hoeks, A.P.; Cleutjens, J.P.; Oostra, R.J.; Daemen, M.J.; van Soest, S.; Reneman, R.S. In patients with pseudoxanthoma elasticum a thicker and more elastic carotid artery is associated with elastin fragmentation and proteoglycans accumulation. In *Ultrasound Med Biol*, England, 2004; Vol. 30, pp. 1041-1048.

56.   Vanakker, O.M.; Leroy, B.P.; Coucke, P.; Bercovitch, L.G.; Uitto, J.; Viljoen, D.; Terry, S.F.; Van Acker, P.; Matthys, D.; Loeys, B.; De Paepe, A. Novel clinico-molecular insights in pseudoxanthoma elasticum provide an efficient molecular screening method and a comprehensive diagnostic flowchart. *Hum Mutat* **2008**, *29*, 205, doi:10.1002/humu.9514.

57.   Mendelsohn, G.; Bulkley, B.H.; Hutchins, G.M. Cardiovascular manifestations of Pseudoxanthoma elasticum. *Arch Pathol Lab Med* **1978**, *102*, 298-302.

58.   Goral, V.; Demir, D.; Tuzun, Y.; Keklikci, U.; Buyukbayram, H.; Bayan, K.; Uyar, A. Pseudoxantoma elasticum, as a repetitive upper gastrointestinal hemorrhage cause in a pregnant woman. *World J Gastroenterol* **2007**, *13*, 3897-3899.

59.   Campens, L.; Vanakker, O.M.; Trachet, B.; Segers, P.; Leroy, B.P.; De Zaeytijd, J.; Voet, D.; De Paepe, A.; De Backer, T.; De Backer, J. Characterization of cardiovascular involvement in pseudoxanthoma elasticum families. In *Arterioscler Thromb Vasc Biol*, United States, 2013; Vol. 33, pp. 2646-2652.

60. D'Marco, L.; Lima-Martínez, M.; Karohl, C.; Chacín, M.; Bermúdez, V. Pseudoxanthoma Elasticum: An Interesting Model to Evaluate Chronic Kidney Disease-Like Vascular Damage without Renal Disease. *Kidney Dis (Basel)* **2020**, *6*, 92-97, doi:10.1159/000505026.

61. Schachner, L.; Young, D. Pseudoxanthoma elasticum with severe cardiovascular disease in a child. *Am J Dis Child* **1974**, *127*, 571-575, doi:10.1001/archpedi.1974.02110230117021.

62. Hosen, M.J.; Lamoen, A.; De Paepe, A.; Vanakker, O.M. Histopathology of Pseudoxanthoma Elasticum and Related Disorders: Histological Hallmarks and Diagnostic Clues. *Scientifica* **2012**, *2012*, 598262, doi:10.6064/2012/598262.

63. Plomp, A.S.; Toonstra, J.; Bergen, A.A.; van Dijk, M.R.; de Jong, P.T. Proposal for updating the pseudoxanthoma elasticum classification system and a review of the clinical findings. *Am J Med Genet A* **2010**, *152a*, 1049-1058, doi:10.1002/ajmg.a.33329.

64. Lacarrubba, F.; Verzì, A.E.; Caltabiano, R.; Micali, G. Dermoscopy of pseudoxanthoma elasticum. *Journal of the American Academy of Dermatology* **2017**, *76*, S69-S70, doi:https://doi.org/10.1016/j.jaad.2016.07.061.

65. Berthin, C.; Phan, A.; Navasiolava, N.; Michalak, S.; Humeau, H.; Grimaux, X.; Martin, L. Dermoscopic phenotype of pseudoxanthoma elasticum skin lesions: a study of 16 patients. *Journal of the European Academy of Dermatology and Venereology* **2019**, *33*, e262-e265, doi:https://doi.org/10.1111/jdv.15534.

66. Kawashima, S.; Togawa, Y.; Miyachi, H.; Matsue, H. Dermoscopic features of pseudoxanthoma elasticum. *Clin Exp Dermatol* **2018**, *43*, 175-179, doi:10.1111/ced.13308.

67. Guérin-Moreau, M.; Leftheriotis, G.; Le Corre, Y.; Etienne, M.; Amode, R.; Hamel, J.F.; Croué, A.; Le Saux, O.; Machet, L.; Martin, L. High-frequency (20-50 MHz) ultrasonography of pseudoxanthoma elasticum skin lesions. *Br J Dermatol* **2013**, *169*, 1233-1239, doi:10.1111/bjd.12545.

68. Mandel, V.D.; Boraldi, F.; Pellacani, G.; Ciardo, S.; Mazzaglia, G.; Farnetani, F. Pseudoxanthoma elasticum and reflectance confocal microscopy: report of two affected young sisters. *Journal of Pediatric and Neonatal Individualized Medicine* **2015**, *4*, 1-4.

69. Persechino, F.; Giordano, D.; Marini, C.D.; Franceschini, C.; Ardigò, M.; Persechino, S. Dermoscopy, Optical Coherence Tomography, and Histological Correlation of

Pseudoxanthoma Elasticum. *Dermatol Pract Concept* **2019**, *9*, 209-210, doi:10.5826/dpc.0903a07.

70. Decani, S.; Varoni, E.M.; Baruzzi, E.; Moneghini, L.; Lodi, G.; Sardella, A. Pseudoxanthoma elasticum of the palate: a case report and a brief review of the literature. *Oral Surg Oral Med Oral Pathol Oral Radiol* **2016**, *121*, e6-9, doi:10.1016/j.oooo.2015.09.010.

71. Marconi, B.; Bobyr, I.; Campanati, A.; Molinelli, E.; Consales, V.; Brisigotti, V.; Scarpelli, M.; Racchini, S.; Offidani, A. Pseudoxanthoma elasticum and skin: Clinical manifestations, histopathology, pathomechanism, perspectives of treatment. *Intractable Rare Dis Res* **2015**, *4*, 113-122, doi:10.5582/irdr.2015.01014.

72. Salles, A.G.; Remigio, A.F.; Moraes, L.B.; Varoni, A.C.; Gemperli, R.; Ferreira, M.C. Pseudoxanthoma Elasticum Treatment with Fractional CO2 Laser. *Plast Reconstr Surg Glob Open* **2014**, *2*, e219, doi:10.1097/gox.0000000000000173.

73. Zsuzsanna;, S.; Erzsébet;, K.; Éva, T. Pseudoxanthoma elasticum kálcium depozitumokkal és exudatív tünetekkel - Pseudoxanthoma elasticum with calcium deporition and exudative (pustular) symptoms. *Bőrgyógyászati és Venerológiai Szemle* **2000**, *76.évf. 6. 241-244*.

74. Gliem, M.; Birtel, J.; Müller, P.L.; Hendig, D.; Faust, I.; Herrmann, P.; Holz, F.G.; Adamus, G.; Charbel Issa, P. Acute Retinopathy in Pseudoxanthoma Elasticum. *JAMA Ophthalmol* **2019**, *137*, 1165-1173, doi:10.1001/jamaophthalmol.2019.2910.

75. De Vilder, E.Y.G.; Hosen, M.J.; Martin, L.; De Zaeytijd, J.; Leroy, B.P.; Ebran, J.M.; Coucke, P.J.; De Paepe, A.; Vanakker, O.M. VEGFA variants as prognostic markers for the retinopathy in pseudoxanthoma elasticum. *Clin Genet* **2020**, *98*, 74-79, doi:10.1111/cge.13751.

76. Terry, S.F.; Uitto, J. Pseudoxanthoma Elasticum. *GeneReviews(®)*, **2001** [updated 2020 Jun 4]. PMID: 20301292.

77. McCreedy, C.A.; Zimmerman, T.J.; Webster, S.F. Management of upper gastrointestinal hemorrhage in patients with pseudoxanthoma elasticum. *Surgery* **1989**, *105*, 170-174.

78. Karam, C.; Soulat, G.; Germain, D.P.; Lacombe, P.; Dubourg, O. Coronary CT angiography for chest pain in pseudoxanthoma elasticum and cardiac intervention management. *J Cardiovasc Comput Tomogr* **2015**, *9*, 238-241, doi:10.1016/j.jcct.2015.02.004.

79. Bartstra, J.W.; de Jong, P.A.; Kranenburg, G.; Wolterink, J.M.; Isgum, I.; Wijsman, A.; Wolf, B.; den Harder, A.M.; Mali, W.; Spiering, W. Etidronate halts systemic arterial calcification in pseudoxanthoma elasticum. *Atherosclerosis* **2020**, *292*, 37-41, doi:10.1016/j.atherosclerosis.2019.10.004.

80. Omarjee, L.; Nitschke, Y.; Verschuere, S.; Bourrat, E.; Vignon, M.D.; Navasiolava, N.; Leftheriotis, G.; Kauffenstein, G.; Rutsch, F.; Vanakker, O.M.; Martin, L. Severe early-onset manifestations of pseudoxanthoma elasticum resulting from the cumulative effects of several deleterious mutations in ENPP1, ABCC6 and HBB: transient improvement in ectopic calcification with sodium thiosulfate. *Br J Dermatol* **2020**, *183*, 367-372, doi:10.1111/bjd.18632.

81. Luo, H.; Li, Q.; Cao, Y.; Uitto, J. Therapeutics Development for Pseudoxanthoma Elasticum and Related Ectopic Mineralization Disorders: Update 2020. *J Clin Med* **2020**, *10*, doi:10.3390/jcm10010114.

82. Arányi, T.; Bacquet, C.; de Boussac, H.; Ratajewski, M.; Pomozi, V.; Fülöp, K.; Brampton, C.N.; Pulaski, L.; Le Saux, O.; Váradi, A. Transcriptional regulation of the ABCC6 gene and the background of impaired function of missense disease-causing mutations. *Front Genet* **2013**, *4*, 27, doi:10.3389/fgene.2013.00027.

83. Huang, J.; Snook, A.E.; Uitto, J.; Li, Q. Adenovirus-Mediated ABCC6 Gene Therapy for Heritable Ectopic Mineralization Disorders. *J Invest Dermatol* **2019**, *139*, 1254-1263, doi:10.1016/j.jid.2018.12.017.

84. Lihachev, A.; Derjabo, A.; Ferulova, I.; Lange, M.; Lihacova, I.; Spigulis, J. Autofluorescence imaging of basal cell carcinoma by smartphone RGB camera. *Journal of Biomedical Optics* **2015**, *20*, 120502.

85. Tamošiūnas, M.; Plorina, E.V.; Lange, M.; Derjabo, A.; Kuzmina, I.; Bļizņuks, D.; Spigulis, J. Autofluorescence imaging for recurrence detection in skin cancer postoperative scars. *J Biophotonics* **2020**, *13*, e201900162, doi:10.1002/jbio.201900162.

86. Secades, C.; O'Connor, B.; Brown, C.; Walpole, M.J.; Skidmore, A.K.; Wang, T. Review of the use of remotely - sensed data for monitoring biodiversity change and tracking progress towards the Aichi Biodiversity Targets : e-book.

87. Li, Y.; Cui, Y.; Zhao, H.; Wang, C.; Liu, X.; Han, J. Pseudoxanthoma elasticum: A review of 86 cases in China. *Intractable & rare diseases research* **2014**, *3*, 75-78.

88. Neldner, K.H. Pseudoxanthoma elasticum. *International journal of dermatology* **1988**, *27*, 98-100.

89. Boraldi, F.; Murro, V.; Lofaro, F.D.; Mucciolo, D.P.; Costa, S.; Pavese, L.; Quaglino, D. Phenotypic Features and Genetic Findings in a Cohort of Italian Pseudoxanthoma Elasticum Patients and Update of the Ophthalmologic Evaluation Score. *Journal of Clinical Medicine* **2021**, *10*, 2710.

90. Letavernier, E.; Kauffenstein, G.; Huguet, L.; Navasiolava, N.; Bouderlique, E.; Tang, E.; Delaitre, L.; Bazin, D.; de Frutos, M.; Gay, C.; Perez, J.; Verpont, MC.; Haymann, JP.; Pomozi, V.; Zoll, J.; Le Saux, O.; Daudon, M.; Leftheriotis, G.; Martin, L. ABCC6 Deficiency Promotes Development of Randall Plaque. *J Am Soc Nephrol* **2018**, *29*, 2337-2347, doi:10.1681/asn.2017101148.

91. Utani, A.; Tanioka, M.; Yamamoto, Y.; Taki, R.; Araki, E.; Tamura, H.; Miyachi, Y. Relationship between the distribution of pseudoxanthoma elasticum skin and mucous membrane lesions and cardiovascular involvement. *J Dermatol* **2010**, *37*, 130-136, doi:10.1111/j.1346-8138.2009.00775.x.

92. Orssaud, C.; Roche, O.; Dufier, J.L.; Germain, D.P. Visual Impairment in Pseudoxanthoma Elasticum: A Survey of 40 Patients. *Ophthalmic Genet* **2015**, *36*, 327-332, doi:10.3109/13816810.2014.886268.

93. Gliem, M.; Müller, P.L.; Birtel, J.; Hendig, D.; Holz, F.G.; Charbel Issa, P. Frequency, Phenotypic Characteristics and Progression of Atrophy Associated With a Diseased Bruch's Membrane in Pseudoxanthoma Elasticum. *Invest Ophthalmol Vis Sci* **2016**, *57*, 3323-3330, doi:10.1167/iovs.16-19388.

94. Risseeuw, S.; Ossewaarde-van Norel, J.; Klaver, C.C.W.; Colijn, J.M.; Imhof, S.M.; van Leeuwen, R. VISUAL ACUITY IN PSEUDOXANTHOMA ELASTICUM. **2019**, *39*, 1580-1587, doi:10.1097/iae.0000000000002173.

95. Lefthériotis, G.; Omarjee, L.; Le Saux, O.; Henrion, D.; Abraham, P.; Prunier, F.; Willoteaux, S.; Martin, L. The vascular phenotype in Pseudoxanthoma elasticum and related disorders: contribution of a genetic disease to the understanding of vascular calcification. *Front Genet* **2013**, *4*, 4, doi:10.3389/fgene.2013.00004.

96. Omarjee, L.; Fortrat, J.O.; Larralde, A.; Pabic, E.L.; Kauffenstein, G.; Laot, M.; Navasiolava, N.; Mention, P.J.; Carrillo Linares, J.L.; Valdivielso, P., Vanakker, OM.; Mahé, G.; Martin, L.; Lefthériotis, G. Internal Carotid Artery Hypoplasia: A New

Clinical Feature in Pseudoxanthoma Elasticum. *J Stroke* **2019**, *21*, 108-111, doi:10.5853/jos.2018.02705.

97. Bartstra, J.W.; Spiering, W.; van den Ouweland, J.M.W.; Mali, W.P.T.M.; Janssen, R.; de Jong, P.A. Increased Elastin Degradation in Pseudoxanthoma Elasticum Is Associated with Peripheral Arterial Disease Independent of Calcification. *Journal of Clinical Medicine* **2020**, *9*, 2771.

98. Hussain, S.; Mubeen, I.; Ullah, N.; Shah, S.; Khan, B.A.; Zahoor, M.; Ullah, R.; Khan, F.A.; Sultan, M.A. Modern Diagnostic Imaging Technique Applications and Risk Factors in the Medical Field: A Review. *Biomed Res Int* **2022**, *2022*, 5164970, doi:10.1155/2022/5164970.

99. Koehler, M.J.; Lange-Asschenfeldt, S.; Kaatz, M. Non-invasive imaging techniques in the diagnosis of skin diseases. *Expert opinion on medical diagnostics* **2011**, *5*, 425-440.

100. Lallas, A.; Argenziano, G. Dermatoscope--the dermatologist's stethoscope. *Indian J Dermatol Venereol Leprol* **2014**, *80*, 493-494, doi:10.4103/0378-6323.144141.

101. Jensen, O.A. Bruch's membrane in pseudoxanthoma elasticum. Histochemical, ultrastructural, and x-ray microanalytical study of the membrane and angioid streak areas. *Albrecht Von Graefes Arch. Klin. Exp. Ophthalmol.* **1977**, *203*, 311-320, doi:10.1007/bf00409836.

102. Walker, E.R.; Frederickson, R.G.; Mayes, M.D. The mineralization of elastic fibers and alterations of extracellular matrix in pseudoxanthoma elasticum. Ultrastructure, immunocytochemistry, and X-ray analysis. *Arch. Dermatol.* **1989**, *125*, 70-76.

103. Machado, T.R.; Leite, I.S.; Inada, N.M.; Li, M.S.; da Silva, J.S.; Andrés, J.; Beltrán-Mir, H.; Cordoncillo, E.; Longo, E. Designing biocompatible and multicolor fluorescent hydroxyapatite nanoparticles for cell-imaging applications. *Materials Today Chemistry* **2019**, *14*, 100211, doi:https://doi.org/10.1016/j.mtchem.2019.100211.

104. Uchida, Y.; Uchida, Y.; Kawai, S.; Kanamaru, R.; Sugiyama, Y.; Tomaru, T.; Maezawa, Y.; Kameda, N. Detection of vulnerable coronary plaques by color fluorescent angioscopy. *JACC Cardiovasc Imaging* **2010**, *3*, 398-408, doi:10.1016/j.jcmg.2009.09.030.

105. Giovannacci, I.; Magnoni, C.; Vescovi, P.; Painelli, A.; Tarentini, E.; Meleti, M. Which are the main fluorophores in skin and oral mucosa? A review with emphasis on clinical applications of tissue autofluorescence. *Arch Oral Biol* **2019**, *105*, 89-98, doi:10.1016/j.archoralbio.2019.07.001.

106. Gutierrez-Cardo, A.; Lillo, E.; Murcia-Casas, B.; Carrillo-Linares, J.L.; Garcia-Arguello, F.; Sanchez-Sanchez, P.; Rodriguez-Morata, A.; Aranda, I.B.; Sanchez-Chaparro, M.A.; Garcia-Fernandez, M.; Valdivielso, P. Skin and Arterial Wall Deposits of 18F-NaF and Severity of Disease in Patients with Pseudoxanthoma Elasticum. *J Clin Med* **2020**, *9*, doi:10.3390/jcm9051393.

107. Khan, M.A.; Beard, J. Peripheral vascular disease in an individual with pseudoxanthoma elasticum. *Eur J Vasc Endovasc Surg* **2007**, *34*, 590-591, doi:10.1016/j.ejvs.2007.04.003.

108. Bartstra, J.W.; de Jong, P.A.; Spiering, W. Accelerated peripheral vascular aging in pseudoxanthoma elasticum - proof of concept for arterial calcification-induced cardiovascular disease. *Aging (Albany NY)* **2019**, *11*, 1062-1064, doi:10.18632/aging.101821.

109. Leftheriotis, G.; Navasiolava, N.; Clotaire, L.; Duranton, C.; Le Saux, O.; Bendahhou, S.; Laurain, A.; Rubera, I.; Martin, L. Relationships between Plasma Pyrophosphate, Vascular Calcification and Clinical Severity in Patients Affected by Pseudoxanthoma Elasticum. *J Clin Med* **2022**, *11*, doi:10.3390/jcm11092588.

9. Bibliography of the candidate's publications

9.1 Publications directly related to this thesis

Farkas K, Bozsányi Sz, Plázár D, Bánvölgyi A, Fésűs L, Anker P, Zakariás S, Lihacova I, Lihachev A, Lange M, Arányi T, Wikonkál NM, Medvecz M, Kiss N. Autofluorescence Imaging of the Skin Is an Objective Non-Invasive Technique for Diagnosing Pseudoxanthoma Elasticum. Diagnostics (Basel). 2021 Feb 8;11(2):260. doi: 10.3390/diagnostics11020260. PMID: 33567497; PMCID: PMC7915757. **IF: 3,992**

Fésűs L, Kiss N, Farkas K, Plázár D, Pálla S, Navasiolava N, Róbert L, Wikonkál NM, Martin L, Medvecz M. Correlation of systemic involvement and presence of pathological skin calcification assessed by ex vivo nonlinear microscopy in Pseudoxanthoma elasticum. Arch Dermatol Res. 2023 Sep;315(7):1897-1908. doi: 10.1007/s00403-023-02557-x. Epub 2023 Feb 27. PMID: 36847829; PMCID: PMC10366029. **IF: 3,0**

Farkas K, Kiss N, Szabó V, Resch M, Vámos R, Borbándy Á, Nagy A, Apor A, Arányi T, Szeri F, Wikonkál NM, Nagy Z, Merkely B, Medvecz M. Pseudoxanthoma elasticumban szenvedő betegek multidiszciplináris ellátása [Multidisciplinary management of patients affected with pseudoxanthoma elasticum]. Orv Hetil. 2022 May 1;163(18):702-711. Hungarian. doi: 10.1556/650.2022.32438. PMID: 35490386. **IF: 0,6**

9.2 Publications indirectly related to this thesis

Bozsányi Sz, Farkas K, Bánvölgyi A, Lőrincz K, Fésűs L, Anker P, Zakariás S, Jobbágy A, Lihacova I, Lihachev A, Lange M, Bliznuks D, Medvecz M, Kiss N, Wikonkál NM. Quantitative Multispectral Imaging Differentiates Melanoma from Seborrheic Keratosis. Diagnostics (Basel). 2021 Jul 22;11(8):1315. doi: 10.3390/diagnostics11081315. PMID: 34441250; PMCID: PMC8392390. **IF: 3,992**

Bozsányi Sz, Varga NN, Farkas K, Bánvölgyi A, Lőrincz K, Lihacova I, Lihachev A, Plorina EV, Bartha Á, Jobbágy A, Kuroli E, Paragh G, Holló P, Medvecz M, Kiss N, Wikonkál NM. Multispectral Imaging Algorithm Predicts Breslow Thickness of Melanoma. J Clin Med. 2021 Dec 30;11(1):189. doi: 10.3390/jcm11010189. PMID: 35011930; PMCID: PMC8745435. **IF: 3,6**

Bozsányi Sz, Boostani M, Farkas K, Hamilton-Meikle P, Varga NN, Szabó B, Vasanits F, Kuroli E, Meznerics FA, Lőrincz K, Holló P, Bánvölgyi A, Wikonkál NM, Paragh G, Kiss N. Optically Guided High-Frequency Ultrasound to Differentiate High-Risk Basal Cell Carcinoma Subtypes: A Single-Centre Prospective Study. J Clin Med. 2023 Nov 3;12(21):6910. doi: 10.3390/jcm12216910. **IF: 3,9**

Kiss N, Farkas K, Tosti G, De Gado F, Bergler-Czop B, Fazia G, Tammaro A, Cantisani C. Photodynamic Therapy with 5-Aminolevulinic Acid Patch for the Treatment of Actinic Keratosis. J Clin Med. 2022 Jun 2;11(11):3164. doi: 10.3390/jcm11113164. **IF: 3,9**

Plázár D, Meznerics FA, Pálla S, Anker P, Farkas K, Bánvölgyi A, Kiss N, Medvecz M. Dermoscopic Patterns of Genodermatoses: A Comprehensive Analysis. Biomedicines. 2023 Oct 6;11(10):2717. doi: 10.3390/biomedicines11102717. **IF: 4,7**

Pálla S, Anker P, Farkas K, Plázár D, Kiss S, Marschalkó P, Szalai Z, Bene J, Hadzsiev K, Maróti Z, Kalmár T, Medvecz M. Co-occurrence of neurofibromatosis type 1 and pseudoachondroplasia - a first case report. BMC Pediatr. 2023 Mar 8;23(1):110. doi: 10.1186/s12887-023-03920-7. **IF: 2,4**

Anker P, Kiss N, Kocsis I, Czemmel É, Becker K, Zakariás S, Plázár D, Farkas K, Mayer B, Nagy N, Széll M, Ács N, Szalai Z, Medvecz M. Report of a Novel ALOX12B Mutation in Self-Improving Collodion Ichthyosis with an Overview of the Genetic Background of the Collodion Baby Phenotype. Life (Basel). 2021 Jun 27;11(7):624. doi: 10.3390/life11070624. **IF: 3,253**

Jobbágy A, Kiss N, Meznerics FA, Farkas K, Plázár D, Bozsányi S, Fésűs L, Bartha Á, Szabó E, Lőrincz K, Sárdy M, Wikonkál NM, Szoldán P, Bánvölgyi A. Emergency Use and Efficacy of an Asynchronous Teledermatology System as a Novel Tool for Early Diagnosis of Skin Cancer during the First Wave of COVID-19 Pandemic. Int J Environ Res Public Health. 2022 Feb 25;19(5):2699. doi: 10.3390/ijerph19052699. **IF: 4,614**

Bozsányi Sz, Czurkó N, Becske M, Kasek R, Lázár BK, Boostani M, Meznerics FA, Farkas K, Varga NN, Gulyás L, Bánvölgyi A, Fehér BÁ, Fejes E, Lőrincz K, Kovács A, Gergely H, Takács S, Holló P, Kiss N, Wikonkál NM, Lázár I. Assessment of Frontal Hemispherical Lateralization in Plaque Psoriasis and Atopic Dermatitis. J Clin Med. 2023 Jun 21;12(13):4194. doi: 10.3390/jcm12134194. **IF: 3,9**

Szalai K, Farkas K, Gergely H, Varga NN, Magyar M, Nagy ZZs, Fésűs L, Bozsányi Sz, Jobbágy A, Medvecz M, Bánvölgyi A, Lőrincz K, Wikonkál NM**, Kiss N.
Magas frekvenciájú ultrahang, optikai koherencia tomográfia és mágnesesrezonancia képalkotás alkalmazási lehetőségei a bőrgyógyászati gyakorlatban [Clinical application of high-frequency ultrasound, optical coherence tomography and magnetic resonance imaging in dermatology]. Bőrgyógyászati és Venerológiai Szemle. 2022 (0006-7768 2064-261X): 98 3 pp 125-132

Farkas K, Kiss N, Szabó V, Lesch B, Szabó A, Maneschg O, Apor A, Nagy AI, Medvecz M. A pseudoxanthoma elasticum örökletes ektópiás mineralizációs zavar komplex multidiszciplináris ellátása [Complex multidisciplinary care of hereditary ectopic mineralization disorder pseudoxanthoma elsticum]. Bőrgyógyászati és Venerológiai Szemle. 2023 (0006-7768 2064-261X): 99 1 p. 39.

Fésűs L, Kiss N, Jobbágy A, Farkas K, Meznerics F, Bozsányi Sz, Bánvölgyi A, Wikonkál NM, Lőrincz K. Innovatív in vivo képalkotó módszerek a bőrgyógyászatban [Innovative in vivo imaging techniques in dermatology]. Bőrgyógyászati és Venerológiai Szemle. 2022 (0006-7768 2064-261X): 98 3 pp 133-141

Jobbágy A, Meznerics FA, Farkas K, Plázár D, Bozsányi Sz, Fésűs L, Róbert L, Schveibert Á, Kuzmanovszki D, Szoldán P, Lőrincz K, Kiss N, Wikonkál NM, Sárdy M, Bánvölgyi A. Teledermatológia: a digitalizáció új korszaka a bőrgyógyászati betegellátásban [Teledermatology: the new era of digitalization in dermatology care]. Bőrgyógyászati és Venerológiai Szemle. 2022 (0006-7768 2064-261X): 98 3 pp 100-107

Medvecz M, Anker P, Pálla S, Plázár D, Farkas K, Kiss N, Becker K. Örökletes ichthyosisok klinikai és genetikai vonatkozásai [Clinical and genetic aspects of inherited ichthyoses]. Bőrgyógyászati és Venerológiai Szemle. 2022 (0006-7768 2064-261X): 98 2 pp 44-54

10. Acknowledgements